Sr. 169

ORNL-5081

Derivation of the Point Spread Function for Zero-Crossing-Demodulated Position-Sensitive Detectors

C. H. Nowlin

OAK RIDGE NATIONAL LABORATORY

OPERATED BY UNION CARBIDE CORPORATION FOR THE ENERGY RESEARCH AND DEVELOPMENT ADMINISTRATION

BLANK PAGE

Printed in the United States of America. Available from
National Technical Information Service
U.S. Department of Commerce
5285 Port Royal Road, Springfield, Virginia 22161
Price: Printed Copy $4.00, Microfiche $2.25

ORNL-5081
UC-32 - Mathematics and Computers

Contract No. W-7405-eng-26

INSTRUMENTATION AND CONTROLS DIVISION

DERIVATION OF THE POINT SPREAD FUNCTION FOR ZERO-CROSSING-DEMODULATED POSITION-SENSITIVE DETECTORS

C. H. Nowlin

JULY 1976

OAK RIDGE NATIONAL LABORATORY
Oak Ridge, Tennessee 37830
operated by
UNION CARBIDE CORPORATION
for the
ENERGY RESEARCH AND DEVELOPMENT ADMINISTRATION

CONTENTS

DERIVATION OF THE POINT SPREAD FUNCTION FOR ZERO-CROSSING-DEMODULATED POSITION-SENSITIVE DETECTORS

C. H. Nowlin

ABSTRACT

This work is a mathematical derivation of a high-quality approximation to the point spread function for position-sensitive detectors (PSDs) that use pulse-shape modulation and crossover-time demodulation. The approximation is determined as a general function of the input signals to the crossover detectors so as to enable later determination of optimum position-decoding filters for PSDs. This work is precisely applicable to PSDs that use either RC or LC transmission line encoders. The effects of random variables, such as charge collection time, in the encoding process are included. In addition, this work presents a new, rigorous method for the determination of upper and lower bounds for conditional crossover-time distribution functions (closely related to first-passage-time distribution functions) for arbitrary signals and arbitrary noise covariance functions.

1. INTRODUCTION

In this work, the point spread function (PSF) for position-sensitive detectors [1–5] (PSDs) is defined and calculated for the first time. This PSF will enable the later determination of impulse responses of optimum position-decoding filters for PSDs. These impulse responses will, in turn, enable the design of optimum position-decoding, pulse-shaping filters for PSDs. In addition, this work provides a generalized, prescribed procedure for the evaluation of existing and propcsed position-decoding filters. It is also productive in evaluating existing and proposed position encoders (e.g., RC position-sensitive proportional counters).

This work is a mathematical derivation of the PSF for a one-dimensional PSD. However, since there is little interaction [3] between the two position-coordinate measurements for two-dimensional PSDs, our PSF can be used for two-dimensional PSDs also. Our theory is developed in general terms so as to be precisely applicable to any PSD that uses either pulse-shape or pulse-epoch modulation together with crossover-time demodulation. This class of PSDs includes those that use a position encoder with an RC transmission line, as well as those that use an encoder with an LC delay line. The effects of thermal noise generated in both the encoder and the preamplifiers are included. The effects of various other random processes, such as electron cloud diffusion [6], in the position encoder are also included. We do not include the effects of correlated thermal noise in our final results, because such noise is likely to be much less important [7, 8] than uncorrelated noise in determining position uncertainty. However, the basic theory does include the effects of correlated noise, and only a few, although difficult, integrals would have to be reevaluated to include such effects in the final results.

As part of the PSF derivation, we derive upper and lower bounds for the joint conditional first-crossover-time distribution for two stochastic processes. Each process is assumed to be the sum of a deterministic function and a purely random process. We derive the bounds in terms of the deterministic and stochastic properties of the processes. We show that our upper and lower bounds converge to the same function with increasing signal-to-noise ratios and that the lower bound is typically a high-quality approximation to the joint first-crossover-time distribution function. The most closely related previous derivations, those for the first-passage-time probability density function [9], are limited to only a single process that must be either a Wiener or a Markov process. In contrast, our derivation is valid for stochastic processes that have any arbitrary autocovariance functions. Our method is indirect but rigorous and versatile. Although we use it in this work to determine the distribution function for the first conditional crossings of the zero level by two stochastic processes, it is also productive when applied to determine the distribution function for the first conditional crossing of nonzero levels by one or two stochastic processes.

In the work that follows, we first define the PSF so that it completely characterizes any PSD. Then, we formulate the PSF calculation so that our results are independent of the particular type of position encoder that is used. Next, an asymptotically correct approximation to the PSF is derived in terms of the deterministic and stochastic properties of the PSD. In the final section, we tell specifically how to use the various equations of this work to calculate the PSF of any PSD.

2. PROBABILISTIC POINT SPREAD FUNCTION

To define the PSD PSF, we first define two position coordinate systems. One of these coordinate systems is defined for the photon source, and the other is defined for the position encoder. Because we will discuss only one-dimensional PSDs, we assume the source is a line source. Then we define y to be the general coordinate along the line source axis and x to be the general coordinate along the position encoder axis. Furthermore, we will add suitable superscripts to y and x to indicate particular values of these coordinates.

We next consider photons that are emitted from the source at position coordinate y_0. Because of random errors in the measurement process, not every photon that is emitted at $y = y_0$ is assigned the same estimated position coordinate by the PSD. We let $\hat{x}_e$ denote the estimated position coordinate that is assigned by the PSD. The circumflex (^) is used to show that the estimated position coordinate is a random variable. Finally, we define the PSD PSF to be the conditional probability density function [10, 11] $P(x_e|y_0)$. The product $P(x_e|y_0)\,dx_e$ is the probability that $x_e \leq \hat{x}_e \leq x_e + dx_e$ under the hypothesis that $\hat{y}_0 = y_0$. The variables x_e and y_0 are the associated arguments [12] of the probability density function. This probabilistic definition of the PSD PSF is in contrast with the deterministic definition of the optical PSF [13, 14].

The PSF that we have defined characterizes a PSD completely. This fact may be proved by combining [11] the definitions of conditional density functions, joint density functions, and marginal density functions to obtain a convolution-like equation for the unconditional probability density function for the estimated position $\hat{x}_e$ when the source density function is given. This convolution-like equation is

$$A(x_e) = \int_{-\infty}^{\infty} P(x_e|y_0)\, T(y_0)\, dy_0. \tag{1}$$

The product $T(y_0)\,dy_0$ is the probability that a photon which is detected by the PSD is emitted from the source between y_0 and $y_0 + dy_0$. The probability density function $T(y_0)$ is obtained by normalizing the source intensity function. The product $A(x_e)\,dx_e$ is the probability that, for the given $T(y_0)$, a detected photon is assigned an estimated position $\hat{x}_e$ such that $x_e \leq \hat{x}_e \leq x_e + dx_e$.

The PSF for a perfect PSD is a delta function. However, for an operating PSD, the PSF is not a delta function; but it is a function with nonzero full width at half maximum. This nonzero full width at half maximum is caused by the interaction of several random processes. To calculate the PSF of an operating PSD, the most important of these random processes are selected and included in a mathematical model of the PSD. For any PSD model, no matter how many random processes are included, we simplify the computation of the overall PSF by separating it into the computation of two simpler conditional probability density functions. We call one the "encoder density function" and the other the "decoder density function."

The decoder density function is $P_d(x_e|x_c, a_1, \ldots, a_n)$. It is determined from the random processes that affect the encoder-generated electronic signal after some position coordinate x_c is encoded into it. This position coordinate is related to but is not necessarily the same as the interaction coordinate of the detected photon. For an RC position-sensitive proportional counter, x_c is the position coordinate where the photon-generated electrons are collected on the resistive center wire. The list of variables $(x_c, a_1, \ldots, a_n)$ is the hypothesis list. The variables in this list are assumed to be fixed parameters when $P_d(x_e|x_c, a_1, \ldots, a_n)$ is calculated. However, the inclusion of a parameter in this list anticipates a random relationship between it and y_0. For the variable x_c, the random relationship can be caused by the random penetration of the encoder by the photon, which is emitted from the source at position coordinate y_0, before the photon interacts with the encoder to produce an electronic signal. The other n parameters, $a_1, \ldots, a_n$, in this hypothesis list represent any other parameters [6] that are anticipated to be random and that affect the shape of the pulse before it is modulated according to x_c. Such variables as charge collection time and photon energy are included in this group. The primary density function describes how all of the random processes, including thermal electronic noise, interact with the position-decoding filters to determine the overall PSF.

The encoder density function is the joint conditional density function $P_e(x_c, a_1, \ldots, a_n|y_0)$. It is determined from the random processes that affect the shape of the encoder-generated electronic pulse before the position coordinate x_c is encoded into it. The source position coordinate y_0 is assumed to be a parameter when $P_e(x_c, a_1, \ldots, a_n|y_0)$ is calculated. If the random variables are independent, $P_e(x_c, a_1, \ldots, a_n|y_0)$ can be factored into simpler conditional probability density functions. The encoder density function is greatly influenced by the particular type of encoder used in the PSD and by the details included in the PSD model, but it is independent of the position-decoding filter.

We use the encoder and decoder density functions together to determine the overall PSF according to the marginal density equation [11]

$$P(x_e|y_0) = \int_{-\infty}^{\infty} \cdots \int_{-\infty}^{\infty} P_d(x_e|x_c, a_1, \ldots, a_n)\, P_e(x_c, a_1, \ldots, a_n|y_0)\, dx_c\, da_1 \ldots da_n \,. \qquad (2)$$

The obstacle to the ready computation of the overall PSF with Eq. (2) is the determination of the decoder density function. The encoder density function is relatively easy to derive or measure. Furthermore, for those PSDs where thermal electronic noise is the principal cause of random errors in position estimation, the decoder density function is a good approximation to the overall PSF. For these reasons, we focus the remainder of this work on the determination of the decoder density function.

We begin the determination of the decoder density function by modeling a simplified PSD in which electronic noise is the only random process. We ignore the details of the encoder because its important properties are described by the encoder density function. All of the variables in the hypothesis list of the decoder density function are treated as parameters in this model. For brevity, we shorten the notation for the decoder density function to $P_d(x_e|x_c)$.

3. MATHEMATICAL MODEL OF THE SIMPLIFIED PSD

To derive $P_d(x_e|x_c)$, we assume an ensemble of PSDs such as the one shown in Fig. 1. All bias voltages, bias currents, and noise sources in the various members of the ensemble are in the steady-state condition.

In the encoder, which is illustrated by an RC position-sensitive proportional counter in Fig. 1, of each member of the ensemble, a photon is detected and a carrier pulse is generated at time t_{0c}. All of the carrier pulses before modulation have the same pulse epoch t_{0c} and are characterized by the same set of parameters $a_1, \ldots, a_n$. Sometime after t_{0c}, the pulse shapes or the apparent pulse epochs are modulated according to x_c, which is the same for each member of the ensemble.

ORNL-DWG 74-3573R4

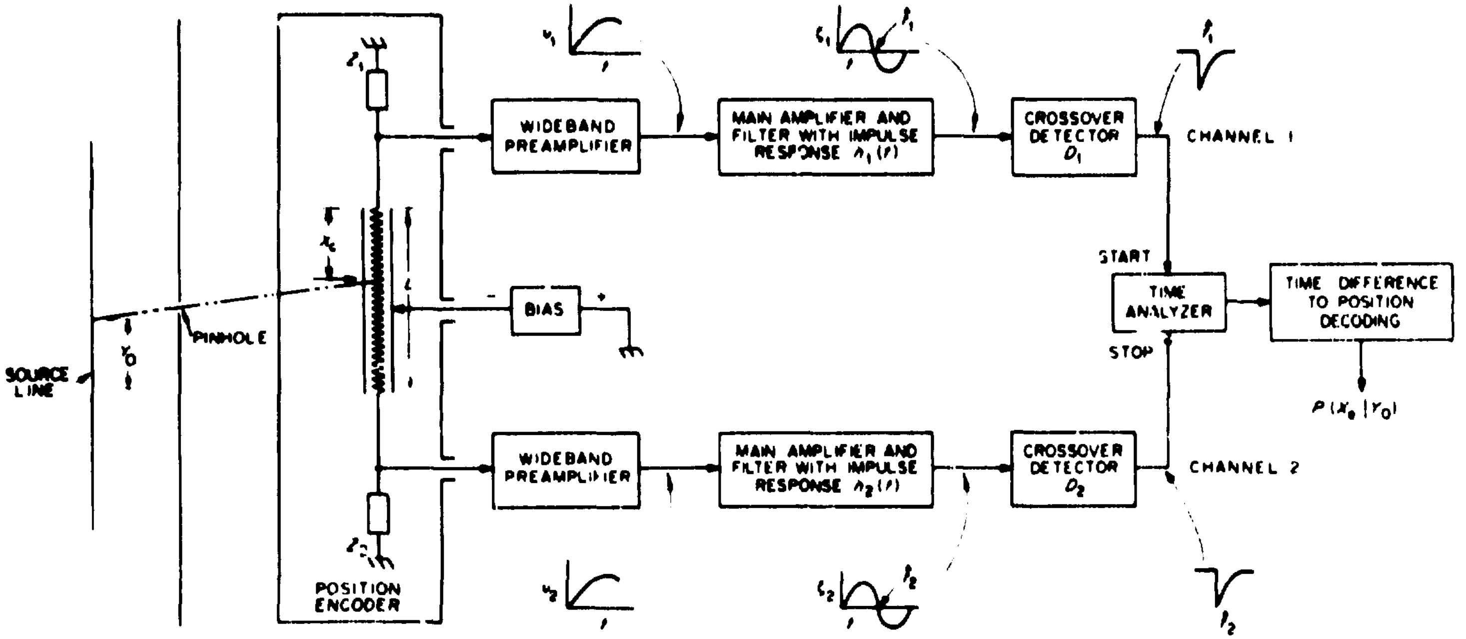

Position Sensitive Detector Model

Fig. 1. The simplified position-sensitive detector.

For a single detected photon, one or more modulated pulses are transmitted from each encoder. Since neither t_{0c} nor x_c is known, two crossover-time measurements must be made to determine either of them from the transmitted pulses. To agree with published descriptions of encoders [1-5], two pulses are shown transmitted from the encoder of Fig. 1 for each detected photon. One pulse is processed in channel 1, and the other pulse is processed in channel 2. A single crossover-time measurement is made in each channel.

The deterministic transmitted pulses are corrupted by additive random noise in the encoder and in the preamplifiers. Hence, from crossover-time measurements of signals received at D_1 and D_2, it is only possible to estimate t_{0c} and x_c. The estimate of t_{0c} is the random variable $\hat{t}_{0c}$, and, as previously stated, the estimate of x_c is the random variable $\hat{x}_c$. To enable the quantification of the accuracy of these estimates, we next mathematically characterize the deterministic signals and the random noise.

We first mathematically characterize the signal and the noise at the outputs of the two wideband preamplifiers, where the signal and the noise have been amplified sufficiently so that additional amplifier noise is not important. At the output of the channel 1 preamplifier, the total observed signal is

$$v_1(x_c, a_1, \ldots, a_n, t_{0c}, t) = \mathrm{v}_1(x_c, a_1, \ldots, a_n, t_{0c}, t) + \gamma_1(t), \tag{3}$$

where $\mathrm{v}_1(x_c, a_1, \ldots, a_n, t_{0c}, t)$ is the deterministic photon-caused pulse, $\gamma_1(t)$ an entirely random [15] zero-mean-noise process, and t the real time. Likewise, at the output of the channel 2 preamplifier, the total observed signal is

$$v_2(x_c, a_1, \ldots, a_n, t_{0c}, t) = \mathrm{v}_2(x_c, a_1, \ldots, a_n, t_{0c}, t) + \gamma_2(t), \tag{4}$$

where $\mathrm{v}_2(x_c, a_1, \ldots, a_n, t_{0c}, t)$ is the deterministic photon-caused pulse and $\gamma_2(t)$ is an entirely random zero-mean-noise process. The functions $\mathrm{v}_1(x_c, a_1, \ldots, a_n, t_{0c}, t)$ and $\mathrm{v}_2(x_c, a_1, \ldots, a_n, t_{0c}, t)$ can be determined from the physical processes of the specific encoder used. However, for this work it is not necessary to know the specific forms of these functions, and we assume they are elsewhere determined [2].

Although the deterministic pulses $\mathrm{v}_1(x_c, a_1, \ldots, a_n, t_{0c}, t)$ and $\mathrm{v}_2(x_c, a_1, \ldots, a_n, t_{0c}, t)$ are the same for all members of the ensemble, the random processes $\gamma_1(t)$ and $\gamma_2(t)$ are different for the various members of the ensemble. These processes include the effects of noise generated in both the encoder and the preamplifiers. Because $\gamma_1(t)$ and $\gamma_2(t)$ are linear combinations of the currents that result from the random motion of many electrons, their joint amplitude probability density function is normal [16]. Therefore, the probability density function for these processes is completely determined [17] from the autovariance functions and the crossvariance functions for $\gamma_1(t)$ and $\gamma_2(t)$. We denote the autovariance function for $\gamma_1(t)$ by $\Gamma_{11}(\tau)$, the autovariance function for $\gamma_2(t)$ by $\Gamma_{22}(\tau)$, and the crossvariance function by $\Gamma_{12}(\tau)$. We assume that $\gamma_1(t)$ and $\gamma_2(t)$ are ergodic. Since, in addition, $\gamma_1(t)$ and $\gamma_2(t)$ are entirely random processes, the variance functions may be determined experimentally as autocorrelation functions and crosscorrelation functions. Alternatively, these variance functions may be calculated from a detailed model of the encoder and the preamplifier according to the defining equation [18]

$$\Gamma_{ij}(\tau) = \langle \gamma_i(t)\, \gamma_j(t+\tau) \rangle \tag{5}$$

where the angle brackets denote ensemble averages, i and j are 1 or 2, and t is unrestricted.

For brevity, we will no longer write the parameters $a_1, \ldots, a_n$ as arguments of the photon-caused pulse. Henceforth, $\mathrm{v}_1(x_c, a_1, \ldots, a_n, t_{0c}, t)$ will at least be contracted to $\mathrm{v}_1(x_c, t_{0c}, t)$, and $\mathrm{v}_2(x_c, a_1, \ldots, a_n, t_{0c}, t)$ will at least be contracted to $\mathrm{v}_2(x_c, t_{0c}, t)$. Furthermore, even these reduced argument

For a single detected photon, one or more modulated pulses are transmitted from each encoder. Since neither t_{0c} nor x_c is known, two crossover-time measurements must be made to determine either of them from the transmitted pulses. To agree with published descriptions of encoders [1–5], two pulses are shown transmitted from the encoder of Fig. 1 for each detected photon. One pulse is processed in channel 1, and the other pulse is processed in channel 2. A single crossover-time measurement is made in each channel.

The deterministic transmitted pulses are corrupted by additive random noise in the encoder and in the preamplifiers. Hence, from crossover-time measurements of signals received at D_1 and D_2, it is only possible to estimate t_{0c} and x_c. The estimate of t_{0c} is the random variable $\hat{t}_{0c}$, and, as previously stated, the estimate of x_c is the random variable $\hat{x}_c$. To enable the quantification of the accuracy of these estimates, we next mathematically characterize the deterministic signals and the random noise.

We first mathematically characterize the signal and the noise at the outputs of the two wideband preamplifiers, where the signal and the noise have been amplified sufficiently so that additional amplifier noise is not important. At the output of the channel 1 preamplifier, the total observed signal is

$$v_1(x_c, a_1, \ldots, a_n, t_{0c}, t) = \mathrm{v}_1(x_c, a_1, \ldots, a_n, t_{0c}, t) + \gamma_1(t), \tag{3}$$

where $\mathrm{v}_1(x_c, a_1, \ldots, a_n, t_{0c}, t)$ is the deterministic photon-caused pulse, $\gamma_1(t)$ an entirely random [15] zero-mean-noise process, and t the real time. Likewise, at the output of the channel 2 preamplifier, the total observed signal is

$$v_2(x_c, a_1, \ldots, a_n, t_{0c}, t) = \mathrm{v}_2(x_c, a_1, \ldots, a_n, t_{0c}, t) + \gamma_2(t), \tag{4}$$

where $\mathrm{v}_2(x_c, a_1, \ldots, a_n, t_{0c}, t)$ is the deterministic photon-caused pulse and $\gamma_2(t)$ is an entirely random zero-mean-noise process. The functions $\mathrm{v}_1(x_c, a_1, \ldots, a_n, t_{0c}, t)$ and $\mathrm{v}_2(x_c, a_1, \ldots, a_n, t_{0c}, t)$ can be determined from the physical processes of the specific encoder used. However, for this work it is not necessary to know the specific forms of these functions, and we assume they are elsewhere determined [2].

Although the deterministic pulses $\mathrm{v}_1(x_c, a_1, \ldots, a_n, t_{0c}, t)$ and $\mathrm{v}_2(x_c, a_1, \ldots, a_n, t_{0c}, t)$ are the same for all members of the ensemble, the random processes $\gamma_1(t)$ and $\gamma_2(t)$ are different for the various members of the ensemble. These processes include the effects of noise generated in both the encoder and the preamplifiers. Because $\gamma_1(t)$ and $\gamma_2(t)$ are linear combinations of the currents that result from the random motion of many electrons, their joint amplitude probability density function is normal [16]. Therefore, the probability density function for these processes is completely determined [17] from the autovariance functions and the crossvariance functions for $\gamma_1(t)$ and $\gamma_2(t)$. We denote the autovariance function for $\gamma_1(t)$ by $\Gamma_{11}(\tau)$, the autovariance function for $\gamma_2(t)$ by $\Gamma_{22}(\tau)$, and the crossvariance function by $\Gamma_{12}(\tau)$. We assume that $\gamma_1(t)$ and $\gamma_2(t)$ are ergodic. Since, in addition, $\gamma_1(t)$ and $\gamma_2(t)$ are entirely random processes, the variance functions may be determined experimentally as autocorrelation functions and crosscorrelation functions. Alternatively, these variance functions may be calculated from a detailed model of the encoder and the preamplifier according to the defining equation [18]

$$\Gamma_{ij}(\tau) = \langle \gamma_i(t)\, \gamma_j(t+\tau) \rangle \tag{5}$$

where the angle brackets denote ensemble averages, i and j are 1 or 2, and t is unrestricted.

For brevity, we will no longer write the parameters $a_1, \ldots, a_n$ as arguments of the photon-caused pulse. Henceforth, $\mathrm{v}_1(x_c, a_1, \ldots, a_n, t_{0c}, t)$ will at least be contracted to $\mathrm{v}_1(x_c, t_{0c}, t)$, and $\mathrm{v}_2(x_c, a_1, \ldots, a_n, t_{0c}, t)$ will at least be contracted to $\mathrm{v}_2(x_c, t_{0c}, t)$. Furthermore, even these reduced argument lists will be varied to meet the conflicting demands of clarity and brevity. Hence, $v_1(x_c, t_{0c}, t)$ may be written simply as v_1 if there is no need to specify the arguments, or it may be written as $v_1(x)$ if we wish to specify that the position variable is x rather than x_c but if we are momentarily unconcerned with t_{0c} and t. In all cases, x with suitable subscripts and superscripts will represent the position variable, and t with suitable subscripts and superscripts will represent the time variable. A similar contraction rule will be implemented for the argument lists of υ_1 and υ_2. Also for brevity, we will frequently omit the time variable when discussing a stochastic process.

As shown in Fig. 1, the stochastic process υ_1 is the input signal to the linear time-invariant filter with impulse response $h_1(t)$, and the stochastic process υ_2 is the input signal to the linear time-invariant filter with impulse response $h_2(t)$. This output signal from the channel 1 filter is

$$\zeta_1(x_c, t_{0c}, t) = \upsilon_1(x_c, t_{0c}, t) * h_1(t) = r_1(x_c, t_{0c}, t) + \phi_1(t) . \quad (6)$$

and the output from the channel 2 filter is

$$\zeta_2(x_c, t_{0c}, t) = \upsilon_2(x_c, t_{0c}, t) * h_2(t) = r_2(x_c, t_{0c}, t) + \phi_2(t) . \quad (7)$$

where the symbol * denotes convolution. Signals r_1 and r_2 are deterministic and are given by

$$r_1(x_c, t_{0c}, t) = v_1(x_c, t_{0c}, t) * h_1(t) \quad (8)$$

and

$$r_2(x_c, t_{0c}, t) = v_2(x_c, t_{0c}, t) * h_2(t) . \quad (9)$$

The argument lists of r_1, r_2, ζ_1, and ζ_2 have been contracted, using the same rules used for v_1 and v_2.

The processes $\phi_1(t)$ and $\phi_2(t)$ are entirely random and are given by

$$\phi_1(t) = \gamma_1(t) * h_1(t) \quad (10)$$

and

$$\phi_2(t) = \gamma_2(t) * h_2(t) . \quad (11)$$

They are stationary and have a normal joint probability density function. The autovariance function for ϕ_1 is [19, 20]

$$\Phi_{11}(\tau) = \int_{-\infty}^{\infty} h_1(\alpha)\, d\alpha \int_{-\infty}^{\infty} h_1(\beta)\, \Gamma_{11}(\tau + \alpha - \beta)\, d\beta . \quad (12)$$

the autovariance function for ϕ_2 is

$$\Phi_{22}(\tau) = \int_{-\infty}^{+\infty} h_2(\alpha)\, d\alpha \int_{-\infty}^{+\infty} h_2(\beta)\, \Gamma_{22}(\tau + \alpha - \beta)\, d\beta . \quad (13)$$

and the crossvariance function for ϕ_1 and ϕ_2 is [21, 22]

$$\Phi_{12}(\tau) = \int_{-\infty}^{+\infty} h_1(\alpha)\, d\alpha \int_{-\infty}^{+\infty} h_2(\beta)\, \Gamma_{12}(\tau + \alpha - \beta)\, d\beta \,. \tag{14}$$

In this fashion, we complete the mathematical characterization of the deterministic and stochastic processes at the outputs of the linear filters. We next consider the crossover-time demodulation process in detail.

To determine t_{0c} and x_c, ζ_1 is demodulated by measuring $\hat{t}_1$, which is the time of the first zero crossing of $\zeta_1(x_c, t_{0c}, t)$ after ζ_1 exceeds a preset amplitude threshold; and ζ_2 is demodulated by measuring $\hat{t}_2$, which is the time of the first zero crossing of $\zeta_2(x_c, t_{0c}, t)$ after ζ_2 exceeds a preset amplitude threshold. Zero-crossing demodulation is used rather than level-crossing demodulation because zero-crossing demodulation is unaffected by changes in pulse amplitude, that is, photon energy. In practice, this demodulation is accomplished by feeding the composite signal ζ_1 into crossover detector D_1 and the composite signal ζ_2 into crossover detector D_2. To ensure zero-crossing demodulation, we require zero bias voltages at the inputs to D_1 and D_2.

The previously mentioned preset amplitude thresholds are the "arming levels" of the crossover detectors. The arming level of D_1 is V_{a1}, and the arming level of D_2 is V_{a2}. We assume that both V_{a1} and V_{a2} are positive. This formulation of zero-crossing demodulation accurately reflects the behavior of crossover detectors that are armed when their input signals first exceed a positive arming level, remain in the armed state until they are triggered disarmed, and emit a standardized output pulse when their input signals next cross zero. Hence, $\hat{t}_1$ is the time when crossover detector D_1 of Fig. 1 is triggered, and $\hat{t}_2$ is the time when crossover detector D_2 of Fig. 1 is triggered.

Because ζ_1 and ζ_2 are stochastic processes, $\hat{t}_1$ and $\hat{t}_2$ are random variables. We define $P_{12}(t_1, t_2|x_c, t_{0c})$ to be the joint conditional probability density function for these random variables for a specified x_c and t_{0c}. We extend our practice of expanding and contracting argument lists of functions to include those of probability density functions. In particular, we will refer to this density function as simply P_{12} when this designation is adequate. In the PSD of Fig. 1, the two random variables $\hat{t}_1$ and $\hat{t}_2$ are reduced to one random variable, $\hat{t}_3 = \hat{t}_2 - \hat{t}_1$, by using the output pulse from D_1 as the start pulse for the time analyzer and the output pulse from D_2 as the stop pulse. This analog computation does not preserve any information about the random variables $\hat{t}_1$ and $\hat{t}_2$. This selective preservation of information is implemented in our mathematical model by changing variables in $P_{12}(t_1, t_2|x_c, t_{0c})$ to obtain $P_{13}(t_1, t_3|x_c, t_{0c})$ and then contracting P_{13} to the marginal density function, $P_3(t_3|x_c)$. Finally, $P_d(x_e|x_c)$ is obtained from P_3 by making the change of variable indicated by the deterministic transformation that relates $\hat{t}_3$ to $\hat{x}_e$.

It is important to remember that this mathematical model is developed for an ensemble of PSDs, each of which processes a single event. When the mathematical equations that are based on this ensemble concept are applied to an operating PSD that processes all events in time sequence, the implicit assumption is made that the cumulative distribution function for $\hat{t}_3$ is ergodic. This assumption is justified if the event rate is small enough so that the number of measured values of $\hat{t}_3$ that are not independent of all other measured values of $\hat{t}_3$ is negligibly small.

The essential density function for the calculation of P_d is P_{12}. Hence we begin the derivation of the decoder function by deriving P_{12} as a function of $\Gamma_{11}(\tau)$, $\Gamma_{12}(\tau)$, $\Gamma_{22}(\tau)$, $v_1(x_c, t_{0c}, t)$, $v_2(x_c, t_{0c}, t)$, $h_1(t)$, and $h_2(t)$.

4. DERIVATION OF THE DECODER DENSITY FUNCTION

4.1 Derivation of P_{12}

4.1.1 General description of the method. To determine the probability density function for the first zero crossing of even a single stochastic process at any time t after the arming of the associated crossover detector, it is necessary to investigate the stochastic process during the entire time interval between the arming of the detector and the time t. The zero-crossing probability density function derived by Rice [23, 24] for stochastic processes with arbitrary autovariance functions is not applicable to this determination because our time interval of investigation is not required to be short enough to cause a one-to-one correspondence between the stochastic process amplitude and time. Hence, to derive P_{12} we use an indirect method.

We begin by shifting our attention from P_{12} to its cumulative distribution function $F_{12}(t_1, t_2|x_c, t_{0c})$. Then, we define an auxiliary cumulative distribution function F which, for a proper choice of parameters, differs from F_{12} by a negligible amount. Then, to determine F, we derive for F an upper bound F_u and a lower bound F_l. We express these bounds in terms of the deterministic and stochastic properties of the PSD. Next, we show that for signal-to-noise ratios greater than 10, the significant nonzero values of $P_{12}(t_1, t_2|x_c, t_{0c})$ are concentrated on a finite range of t_1, t_2. For this finite range, the difference between F_l and F is negligible for signal-to-noise ratios greater than 10. Finally, we conclude that either $P_{12} = 0$ or $P_{12} = \partial^2 F_l/\partial t_1 \partial t_2$, according to the values of t_1 and t_2 that are specified. We begin our derivation with several definitions that lead to the definition of F and to the relationship $F_{12} = F$.

4.1.2 Definition of F and its equivalence to F_{12}. To simplify further discussions, we first define some important time variables that depend on the characteristics of the deterministic functions $r(t)$. We define these variables verbally here and define them graphically in Fig. 2. In Fig. 2 and throughout this work, the

ORNL-DWG 74-3576

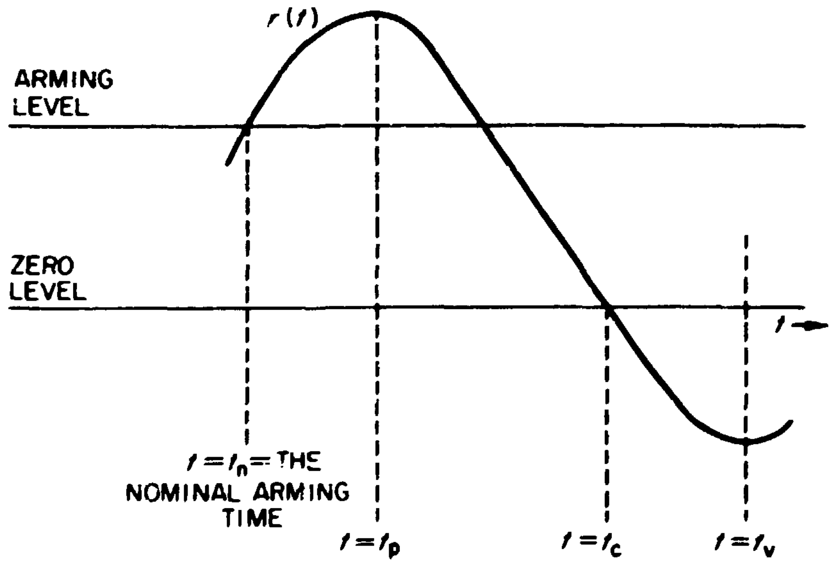

Fig. 2. A sketch of those portions of $r(t)$ that are necessary to illustrate the definitions of some important values of t.

absence of a numerical subscript on a function or variable that normally has the subscript 1 or 2 means that both of the numerically subscripted functions or variables are implied; for example, $r(t)$ is in lieu of $r_1(t)$ or $r_2(t)$. We first define t_{n1}, which is the nominal arming time of D_1, as the smallest value of t for which $r_1(t) = V_{a1}$. We define t_{n2}, which is the nominal arming time of D_2, as the smallest value of t for which $r_2(t) = V_{a2}$. We next define t_{p1} as the time when $r_1(t)$ reaches its first maximum after $t = t_{n1}$. We define t_{p2} as the time when $r_2(t)$ reaches its first maximum after $t = t_{n2}$. We then define t_{c1} as the time when $r_1(t)$ first crosses zero after $t = t_{p1}$. In a similar fashion, we define t_{c2} as the time when $r_2(t)$ first crosses zero after $t = t_{p2}$. Finally, we define t_{v1} as the time when $r_1(t)$ reaches its first minimum after $t = t_{c1}$, and we define t_{v2} as the time when $r_2(t)$ reaches its first minimum after $t = t_{c2}$.

To begin the definition of F, we define the time interval T_1 by its beginning t_{a1} and its ending t_1, and we say that t is in T_1 if and only if $t_{a1} \leq t \leq t_1$. We also define the time interval T_2 by its beginning t_{a2} and its ending t_2, and we say that t is in T_2 if and only if $t_{a2} \leq t \leq t_2$. Except that $t_{a1} \leq t_1$ and $t_{a2} \leq t_2$, the values of t_{a1}, t_1, t_{a2}, and t_2 are not restricted yet.

Next, attention is focused on the behavior of the stochastic processes $\zeta_1(t)$ and $\zeta_2(t)$ during T_1 and T_2, respectively. Each member of the PSD ensemble is characterized by four additional nonnegative integer random variables. These random variables are $\hat{n}_{d1}$, $\hat{n}_{d2}$, $\hat{n}_{u1}$, and $\hat{n}_{u2}$. They are defined as follows:

1. $\hat{n}_{d1}$ is the total number of "downcrossings" of $\zeta_1(t)$ within the interval T_1 for one randomly chosen member of the PSD ensemble. A downcrossing occurs for $\zeta_1(t)$ when $\zeta_1(t) = 0$ and $\dot{\zeta}_1(t) < 0$ [24].

2. $\hat{n}_{u1}$ is the total number of "upcrossings" of $\zeta_1(t)$ within the interval T_1 for one randomly chosen member of the PSD ensemble. An upcrossing occurs for $\zeta_1(t)$ when $\zeta_1(t) = 0$ and $\dot{\zeta}_1(t) > 0$.

3. $\hat{n}_{d2}$ is the total number of downcrossings of $\zeta_2(t)$ within the interval T_2 for one randomly chosen member of the PSD ensemble. A downcrossing occurs for $\zeta_2(t)$ when $\zeta_2(t) = 0$ and $\dot{\zeta}_2(t) < 0$.

4. $\hat{n}_{u2}$ is the total number of upcrossings of $\zeta_2(t)$ within the interval T_2 for one randomly chosen member of the PSD ensemble. An upcrossing occurs for $\zeta_2(t)$ when $\zeta_2(t) = 0$ and $\dot{\zeta}_2(t) > 0$.

The stochastic process $\dot{\zeta}(t)$ is the time derivative of $\zeta(t)$. The joint discrete probability density function for $\hat{n}_{d1}$, $\hat{n}_{d2}$, $\hat{n}_{u1}$, $\hat{n}_{u2}$ is $P_c(n_{d1}, n_{d2}, n_{u1}, n_{u2})$. We do not consider tangencies of $\zeta(t)$ in the above definitions because the average number of tangencies of $\zeta(t)$ in any finite time interval is zero [25, 26].

Next, we define $F(t_1, t_2|x_c, t_{0c})$ to be the total probability for the occurrence of the event $\{\hat{n}_{d1} \geq 1, \hat{n}_{d2} \geq 1\}$ without regard for the value of $\hat{n}_{u1}$ or $\hat{n}_{u2}$; that is,

$$F(t_1, t_2|x_c, t_{0c}) = \sum_{n_{d1}=1}^{\infty} \sum_{n_{d2}=1}^{\infty} \sum_{n_{u1}=0}^{\infty} \sum_{n_{u2}=0}^{\infty} P_c(n_{d1}, n_{d2}, n_{u1}, n_{u2}). \tag{15}$$

Because the probability of any zero crossings by a stochastic process during a time interval that ends before it begins is certainly zero, $F = 0$ for $t_1 \leq t_{a1}$ or $t_2 \leq t_{a2}$. In addition, if r_1 and r_2 (or their representative sequence functions [27]) are absolutely continuous, then, for a fixed t_{a1} and t_{a2}, F is a continuous monotonic increasing function of t_1 and t_2. Furthermore, $F(\infty, \infty|x_c, t_{0c}) = 1$, because $\zeta_1(t)$ and $\zeta_2(t)$ are certain to cross zero one or more times in any infinitely long time interval. Hence, for a fixed t_{a1} and t_{a2}, $F(t_1, t_2|x_c, t_{0c})$ is a cumulative distribution function. Finally, because D_1 and D_2 have positive arming levels and are triggered by downcrossings only, F is the same as F_{12} if the probability is 1 for the occurrence of the event E_a, which is defined as occurring if and only if D_1 is armed but not subsequently triggered before $t = t_{a1}$ and D_2 is armed but not subsequently triggered before $t = t_{a2}$.

To select t_{a1} and t_{a2} so that it is almost certain that the event E_a occurs, we assume that no D_1 or D_2 in the ensemble is triggered before the carrier pulse is generated in the encoder; that is, we assume $F_{12}(t_{0c}, t_{0c}|x_c, t_{0c}) = 0$. This assumption is justified by the common practice of adjusting crossover detectors so that they are not triggered by noise alone during an arbitrarily long observation period. In addition, we have elsewhere modified[1] the techniques that are developed in this work for zero-crossing probability density functions and applied these modified techniques to determine a lower bound for the probability that D_1 becomes armed but is not subsequently triggered between $t = t_{0c}$ and $t = t_{p1}$ and D_2 becomes armed but is not subsequently triggered between $t = t_{0c}$ and $t = t_{p2}$. For typical experimental conditions [where the arming levels V_{a1} and V_{a2} are more than 10 times the rms noise levels at D_1 and D_2, respectively, and $r_1(t_{p1}) \geqslant 2V_{a1}$ and $r_2(t_{p2}) \geqslant 2V_{a2}$], we have calculated that this probability is greater than $1 - \epsilon$, where $\epsilon = 10^{-10}$. Because the probability that E_a does not occur is so extremely small for typical experimental conditions, we conclude that

$$F_{12} = F \tag{16}$$

if $t_{a1} = t_{p1}$ and $t_{a2} = t_{p2}$.

Having defined F and shown its relationship to F_{12}, we next define upper and lower bounds for F in terms of stochastic averages which, in turn, are later derived as functions of the deterministic and stochastic properties of $\zeta(t)$.

4.1.3 Definition of upper and lower bounds for F. There are many possible upper and lower bounds for F. To be useful in our work, the upper and lower bounds we choose must have two important characteristics. First, they must be expressible in terms of the deterministic and stochastic properties of $\zeta_1(t)$ and $\zeta_2(t)$. Second, when these bounds are expressed as functions of the deterministic and stochastic properties of $\zeta_1(t)$ and $\zeta_2(t)$, the bounds must converge rapidly and monotonically with increasing signal-to-noise ratios so as to define F for typical operating PSDs. We denote our specially chosen upper bound of F by F_u and our specially chosen lower bound by F_l. In this section, we select these functions and then show that our selection for F_u does indeed define an upper bound for F and that our selection for F_l does indeed define a lower bound for F.

We first select F_u to be

$$F_u = \langle \hat{n}_{d1} \hat{n}_{d2} \rangle \tag{17}$$

$$= \sum_{n_{d1}=0}^{\infty} \sum_{n_{d2}=0}^{\infty} \sum_{n_{u1}=0}^{\infty} \sum_{n_{u2}=0}^{\infty} n_{d1} n_{d2} P_c(n_{d1}, n_{d2}, n_{u1}, n_{u2}) . \tag{18}$$

Equation (18) is obtained from Eq. (17) by applying the techniques [28] for the computation of ensemble averages of functions of discrete random variables. Since multiplication by $n_{d1} n_{d2}$ makes every nonzero term in Eq. (18) greater than or equal to the corresponding term in Eq. (15), F_u is an upper bound[2] of F.

Next, we select F_l to be

$$F_l = B - C . \tag{19}$$

---

1. Work not published.
2. For a single stochastic process and a positive arming level, a suitable upper bound for the zero-crossing-time cumulative distribution function is $\langle \hat{n}_d \rangle$.

where

$$B = \langle \hat{n}_{d1}\hat{n}_{d2} \rangle - \langle \hat{n}_{u1}\hat{n}_{d2} \rangle - \langle \hat{n}_{d1}\hat{n}_{u2} \rangle + \langle \hat{n}_{u1}\hat{n}_{u2} \rangle . \tag{20}$$

$$C = \int_{-\infty}^{0} \int_{-\infty}^{0} W_a(\alpha_1, \alpha_2)\, d\alpha_1 d\alpha_2 . \tag{21}$$

$W_a(\alpha_1, \alpha_2)$ is the joint probability density function for α_1 and α_2, $\alpha_1 = \zeta_1(t_{a1})$, and $\alpha_2 = \zeta_2(t_{a2})$.

To prove that F_l is a lower bound for F, first B is calculated from Eq. (20) as

$$B = \sum_{n_{d1}=0}^{\infty} \sum_{n_{d2}=0}^{\infty} \sum_{n_{u1}=0}^{\infty} \sum_{n_{u2}=0}^{\infty} N(n_{d1}, n_{d2}, n_{u1}, n_{u2}) . \tag{22}$$

where

$$N(n_{d1}, n_{d2}, n_{u1}, n_{u2}) = (n_{d1} - n_{u1})(n_{d2} - n_{u2}) P_c(n_{d1}, n_{d2}, n_{u1}, n_{u2}) .$$

Since upcrossings and downcrossings must alternate, P_c is zero unless $n_{u1} = n_{d1}$ and $n_{u2} = n_{d2}$, or $n_{u1} = n_{d1}$ and $n_{u2} = n_{d2} \pm 1$, or $n_{u1} = n_{d1} \pm 1$ and $n_{u2} = n_{d2}$, or $n_{u1} = n_{d1} \pm 1$ and $n_{u2} = n_{d2} \pm 1$. By using this property of P_c together with Eq. (22), we find, after discarding the negative terms that result from the expansion of Eq. (22), that

$$B \leq U + V , \tag{23}$$

where

$$U = \sum_{n_{d1}=0}^{\infty} \sum_{n_{d2}=0}^{\infty} P_c(n_{d1}, n_{d2}, n_{d1} - 1, n_{d2} - 1) \tag{24}$$

and

$$V = \sum_{n_{d1}=0}^{\infty} \sum_{n_{d2}=0}^{\infty} P_c(n_{d1}, n_{d2}, n_{d1} + 1, n_{d2} + 1) . \tag{25}$$

Because $\hat{n}_{u1}$ and $\hat{n}_{u2}$ are nonnegative integers, $P_c(0, 0, -1, -1)$, $P_c(n_{d1}, 0, n_{d1} - 1, -1)$, and $P_c(0, n_{d2}, -1, n_{d2} - 1)$ are all zero. For this reason, the lower limits for both n_{d1} and n_{d2} of Eq. (24) can be changed from 0 to 1 with no change in the value of U. Then, after changing these limits, Eq. (24) becomes the same as Eq. (15) except that the values assumed by n_{u1} and n_{u2} in Eq. (24) are a subset of the values assumed by n_{u1} and n_{u2} in Eq. (15). Hence, since P_c is always positive,

$$U \leq F \tag{26}$$

is obtained immediately.

To continue the proof that F_l is a lower bound for F, we note that the occurrence of the event $\{\hat{n}_{u1} = \hat{n}_{d1} + 1, \hat{n}_{u2} = \hat{n}_{d2} + 1\}$ requires the occurrence of the event $\{\zeta_1(t_{a1}) \leq 0, \zeta_2(t_{a2}) < 0\}$, but not vice versa. Hence, we conclude that V is less than or equal to the total probability that the event $\{\zeta_1(t_{a1}) < 0, \zeta_2(t_{a2}) < 0\}$ occurs without regard to the values of $\hat{n}_{d1}$ or $\hat{n}_{d2}$. This conclusion, together with Eq. (21), yields

$$V \leq C. \tag{27}$$

By combining Eqs. (19), (23), (26), and (27),

$$F_l \leq F \tag{28}$$

is finally obtained. Hence, Eq. (19) does, indeed, define a lower bound[2] for F. This lower bound complements the upper bound defined by Eq. (17).

In this section, we have defined upper and lower bounds for F which are functions of $\langle \hat{n}_{d1}\hat{n}_{d2}\rangle$, $\langle \hat{n}_{d1}\hat{n}_{u2}\rangle$, $\langle \hat{n}_{u1}\hat{n}_{d2}\rangle$, $\langle \hat{n}_{u1}\hat{n}_{u2}\rangle$, and W_a. In the next section we will continue our derivation of the primary density function by deriving $\langle \hat{n}_{d1}\hat{n}_{d2}\rangle$, $\langle \hat{n}_{d1}\hat{n}_{u2}\rangle$, $\langle \hat{n}_{u1}\hat{n}_{d2}\rangle$, $\langle \hat{n}_{u1}\hat{n}_{u2}\rangle$, W_a, and, as a result, F_l and F_u as functions of the deterministic signals $r(t)$ and the auto- and crossvariance functions for $\phi(t)$.

4.1.4 Derivation of F_l and F_u as functions of the deterministic and stochastic properties of $\zeta(t)$. In this section, we first derive $\langle \hat{n}_{d1}\hat{n}_{d2}\rangle$, $\langle \hat{n}_{u1}\hat{n}_{d2}\rangle$, $\langle \hat{n}_{d1}\hat{n}_{u2}\rangle$, and $\langle \hat{n}_{u1}\hat{n}_{u2}\rangle$ as functions of $r(t)$, $\Phi_{11}(\tau)$, $\Phi_{12}(\tau)$, and $\Phi_{22}(\tau)$. Cramer and Leadbetter [25, 26] have rigorously derived such ensemble averages as $\langle \hat{n}_{d1}\rangle$, $\langle \hat{n}_{u1}\rangle$, etc., for a single stochastic process. The presentation of their derivation modified for two stochastic processes is beyond the scope of this paper. However, using Cramer and Leadbetter's published derivation as a model, we have completed such a modified derivation. As a result of this derivation, we find that all of the ensemble averages that are needed in F_l and F_u can be represented by the generic function

$$\langle \hat{n}_{i1}\hat{n}_{j2}\rangle = \int_{t_{a1}}^{t_1}\int_{t_{a2}}^{t_2} P_{ij}(v_1, v_2)\, dv_2 dv_1 \, . \tag{29}$$

with

$$P_{ij}(t_1, t_2) = \iint_{R_{ij}} |\dot{\zeta}_1(t_1)||\dot{\zeta}_2(t_2)|\, W[\zeta_1(t_1) = 0, \zeta_2(t_2) = 0, \dot{\zeta}_1(t_1), \dot{\zeta}_2(t_2)]\, d\dot{\zeta}_1 d\dot{\zeta}_2 \, . \tag{30}$$

where i and j represent either d or u depending on the product that is averaged over the ensemble and where $W[\zeta_1(t_1), \zeta_2(t_2), \dot{\zeta}_1(t_1), \dot{\zeta}_2(t_2)]$ is the time-dependent joint amplitude probability density function for the indicated random variables. The various boundaries for the region R_{ij} and the values assigned $\dot{\zeta}_1$ and $\dot{\zeta}_2$ in Eq. (30) result from the equivalence of a downcrossing with the condition $\zeta = 0, \dot{\zeta} < 0$, and the equivalence of an upcrossing with the condition $\zeta = 0, \dot{\zeta} > 0$. To calculate $\langle \hat{n}_{d1}\hat{n}_{d2}\rangle$, first P_{dd} is obtained by evaluating the double integral of Eq. (30) over the region R_{dd}, which, because of the way we have defined a downcrossing, is the quadrant of the $\dot{\zeta}_1, \dot{\zeta}_2$ plane defined by $\dot{\zeta}_1 < 0, \dot{\zeta}_2 < 0$. Then, $\langle \hat{n}_{d1}\hat{n}_{d2}\rangle$ is obtained by using P_{dd} as the integrand in Eq. (29). Similarly, $\langle \hat{n}_{d1}\hat{n}_{u2}\rangle$ is calculated from P_{du}, which is obtained by evaluating the double integral of Eq. (30) over the region R_{du} (this is the quadrant defined by $\dot{\zeta}_1 < 0$, $\dot{\zeta}_2 > 0$). The ensemble average $\langle \hat{n}_{u1}\hat{n}_{d2}\rangle$ is calculated from P_{ud}, which is obtained by evaluating the double integral of Eq. (30) over the region R_{ud} (this is the quadrant defined by $\dot{\zeta}_1 > 0, \dot{\zeta}_2 < 0$). Finally, $\langle \hat{n}_{u1}\hat{n}_{u2}\rangle$

2. For a single stochastic process and a positive arming level, a suitable lower bound for the zero-crossing-time cumulative distribution function is $\langle \hat{n}_d\rangle - \langle \hat{n}_u\rangle$.

is calculated from P_{uu}, which is obtained by evaluating the double integral of Eq. (30) over the region R_{uu} (this is the quadrant defined by $\dot{\zeta}_1 > 0, \dot{\zeta}_2 > 0$).

In matrix notation, the probability density function W is given by [29]

$$W(\zeta_1, \zeta_2, \dot{\zeta}_1, \dot{\zeta}_2) = (2\pi)^{-2} \Delta^{-1/2} \exp[-(\widetilde{Z} - \widetilde{R})M(Z - R)/2] , \tag{31}$$

where the tilde symbol is used to indicate the transpose of a matrix; $\widetilde{Z}$ is the row matrix $[\zeta_1(t_1), \zeta_2(t_2), \dot{\zeta}_1(t_1), \dot{\zeta}_2(t_2)]$; $\widetilde{R}$ is the row matrix $[r_1(t_1), r_2(t_2), \dot{r}_1(t_1), \dot{r}_2(t_2)]$; $\dot{r}(t)$ is the time derivative of $r(t)$; $M = K^{-1}$; K is the covariance matrix for the random variables $\phi_1(t_1)$, $\phi_2(t_2)$, $\dot{\phi}_2(t_1)$, and $\dot{\phi}_2(t_2)$; and Δ is the determinant of K.

The element of the matrix K in the ith row and jth column is k_{ij}. Since K is symmetric, only ten matrix elements are needed to specify K. With $\tau_{21} = t_2 - t_1$, the elements in the first row are given by [30] $k_{11} = \Phi_{11}(0)$, $k_{12} = \Phi_{12}(\tau_{21})$, $k_{13} = 0$, and $k_{14} = [d\Phi_{12}(\tau)/d\tau]_{\tau=\tau_{21}}$. The needed elements in the second row are given by $k_{22} = \Phi_{22}(0)$, $k_{23} = -k_{14}$, and $k_{24} = 0$. The needed elements in the third row are given by $k_{33} = [-d^2\Phi_{11}(\tau)/d\tau^2]_{\tau=0}$ and $k_{34} = [-d^2\Phi_{12}(\tau)/d\tau^2]_{\tau=\tau_{21}}$. Finally, the last element is $k_{44} = [-d^2\Phi_{22}(\tau)/d\tau^2]_{\tau=0}$.

Until this point we have assumed that $\gamma_1(t)$ and $\gamma_2(t)$ [and, hence, $\phi_1(t)$ and $\phi_2(t)$] are correlated because this assumption complicated the derivations only slightly and because these processes are indeed correlated. They are correlated because components of both processes have a common origin in the encoder and because noise generated in the preamplifier of channel 1 is coupled via the encoder into the preamplifier of channel 2, and vice versa. However, because continued assumption of correlation will cause considerable difficulty in the evaluation of the integrals for Eq. (30) and because we expect the effects of correlated noise to be much less important than the effects of uncorrelated noise in determining the distribution of $\hat{x}_e$, we will assume that $\Gamma_{12}(\tau) \equiv 0 \equiv \Phi_{12}(\tau)$ for the remainder of this work. As a result of this assumption, the elements of the matrix M are zero except the diagonal elements. The diagonal elements are given by $m_{11} = 1/k_{11}$, $m_{22} = 1/k_{22}$, $m_{33} = 1/k_{33}$, and $m_{44} = 1/k_{44}$. Use of this specification for M in Eq. (31) yields

$$W(\zeta_1, \zeta_2, \dot{\zeta}_1, \dot{\zeta}_2) = (2\pi)^{-2} [\Delta \exp(u_1 + u_2)]^{-1/2} , \tag{32}$$

where

$$u_1 = r_1^2(t_1)/k_{11} + \dot{r}_1^2(t_1)/k_{33} + [\zeta_1^2 - 2\zeta_1 r_1(t_1)]/k_{11} + [\dot{\zeta}_1^2 - 2\dot{\zeta}_1 \dot{r}_1(t_1)]/k_{33} ,$$

$$u_2 = r_2^2(t_2)/k_{22} + \dot{r}_2^2(t_2)/k_{44} + [\zeta_2^2 - 2\zeta_2 r_2(t_2)]/k_{22} + [\dot{\zeta}_2^2 - 2\dot{\zeta}_2 \dot{r}_2(t_2)]/k_{44} ,$$

and

$$\Delta = k_{11}k_{22}k_{33}k_{44} .$$

After substituting Eq. (32) into Eq. (30) and performing the indicated integrations [31], we obtain

$$P_{dd}(t_1, t_2) = H(t_1, t_2)\, G[-y_1(t_1)]\, G[-y_2(t_2)] , \tag{33}$$

$$P_{du}(t_1, t_2) = -H(t_1, t_2)\, G[-y_1(t_1)]\, G[+y_2(t_2)] . \tag{34}$$

$$P_{ud}(t_1, t_2) = -H(t_1, t_2)\,G[+y_1(t_1)]\,G[-y_2(t_2)] \ . \tag{35}$$

$$P_{uu}(t_1, t_2) = H(t_1, t_2)\,G[+y_1(t_1)]\,G[+y_2(t_2)] \ . \tag{36}$$

where

$$H(t_1, t_2) = H_1(t_1)\,H_2(t_2) \ ,$$

$$H_1(t_1) = -(2\pi k_{11})^{-1/2}\,\dot{r}_1(t_1)\exp[-u_3(t_1)/2] \ ,$$

$$H_2(t_2) = -(2\pi k_{22})^{-1/2}\,\dot{r}_2(t_2)\exp[-u_4(t_2)/2] \ ,$$

$$u_3(t_1) = r_1^{\,2}(t_1)/k_{11} \ ,$$

$$u_4(t_2) = r_2^{\,2}(t_2)/k_{22} \ ,$$

$$G(y) = 0.5\,[1 + \mathrm{erf}\,y + \pi^{-1/2}\,y^{-1}\,\exp(-y^2)] \ ,$$

$$y_1(t_1) = \dot{r}_1(t_1)(2k_{33})^{-1/2} \ ,$$

$$y_2(t_2) = \dot{r}_2(t_2)(2k_{44})^{-1/2} \ ,$$

and erf is the error function. In addition, there is the very useful identity

$$G(y) + G(-y) \equiv 1 \ . \tag{37}$$

Equations (33) – (36) are used in Eq. (29) to yield expressions for $\langle \hat{n}_{d1}\hat{n}_{d2}\rangle$, $\langle \hat{n}_{d1}\hat{n}_{u2}\rangle$, $\langle \hat{n}_{u1}\hat{n}_{d2}\rangle$, and $\langle \hat{n}_{u1}\hat{n}_{u2}\rangle$ as functions of the deterministic and stochastic properties of $\zeta(t)$. Then these expressions are used according to Eq. (17) to completely determine F_u and according to Eqs. (19) and (20) to partially determine F_l. The results of such use are

$$F_u = \int_{t_{a2}}^{t_2}\int_{t_{a1}}^{t_1} G[-y_1(\nu_1)]\,G[-y_2(\nu_2)]\,H(\nu_1, \nu_2)\,d\nu_1 d\nu_2 \ . \tag{38}$$

$$B = \int_{t_{a2}}^{t_2}\int_{t_{a1}}^{t_1} H(\nu_1, \nu_2)\,d\nu_1 d\nu_2 \ . \tag{39}$$

To complete the determination of F_l, C [which is defined by Eq. (21)] is next derived as a function of the deterministic and stochastic properties of $\zeta(t)$. The probability density function W_a is given by [29]

$$W_a(\alpha_1, \alpha_2) = (2\pi)^{-1}\,\Delta_a^{-1/2}\exp[-(\widetilde{\mathbf{Z}}_a - \widetilde{\mathbf{R}}_a)\mathbf{M}_a(\mathbf{Z}_a - \mathbf{R}_a)/2] \ . \tag{40}$$

where $\widetilde{\mathbf{Z}}_a$ is the row matrix $[\alpha_1, \alpha_2]$, $\widetilde{\mathbf{R}}_a$ is the row metrix $[r_1(t_{a1}), r_2(t_{a2})]$. $\mathbf{M}_a = \mathbf{C}^{-1}$, $\mathbf{C}$ is the covariance matrix for the random variables α_1 and α_2, and Δ_a is the determinant of $\mathbf{C}$. The matrix $\mathbf{C}$ is symmetric, and $c_{11} = k_{11}$, $c_{12} = \Phi_{12}(t_{a2} - t_{a1})$, and $c_{22} = k_{22}$. For $\Phi_{12}(\tau) \equiv 0$, the use of Eq. (40) in Eq. (21) yields

$$C = 0.25\, \mathrm{erfc}[r_1(t_{a1})(2k_{11})^{-1/2}]\, \mathrm{erfc}[r_2(t_{a2})(2k_{22})^{-1/2}] \,. \tag{41}$$

where erfc is the complementary error function. Equations (39) and (41), when combined according to Eq. (19), completely determine F_l as a function of the deterministic and stochastic properties of $\zeta(t)$. We continue our work by using F_l and F_u to determine F.

4.1.5 Calculation of P_{12} for signal-to-noise ratios greater than 10.

4.1.5.1 *General discussion of this calculation.* In the previous section, we derived F_l and F_u as functions of $r(t)$ and $\Phi(\tau)$. For those derivations, we did not restrict t_{a1} or t_{a2}. Now, however, to make F_l and F_u useful in the calculation of P_{12}, we require that $t_{a1} = t_{p1}$ and $t_{a2} = t_{p2}$. In addition, to simplify further discussions in this section, we define the region M of the t_1, t_2 plane as that part of the plane where $t_{p1} < t_1 < t_{v1}$ and $t_{p2} < t_2 < t_{v2}$. For the same reason, we define the region $\bar{M}$ as the remainder of the t_1, t_2 plane. Furthermore, we define the signal-to-noise ratio of channel 1 as

$$SN_1 = r_1(t_{p1})/\sqrt{k_{11}} \tag{42}$$

and the signal-to-noise ratio of channel 2 as

$$SN_2 = r_2(t_{p2})/\sqrt{k_{22}} \,. \tag{43}$$

With these definitions and the requirement that $t_{a1} = t_{p1}$ and $t_{a2} = t_{p2}$, we will next prove that the cumulative probability of the ordered pair of random variables $(\hat{t}_1, \hat{t}_2)$ being in $\bar{M}$ converges monotonically to 0 as SN_1 and SN_2 increase without bound. Then, we prove that on M, F converges monotonically and uniformly to F_l as SN_1 and SN_2 increase without bound. After finishing these convergence proofs, we will discuss the effects of finite SN_1 and SN_2 on the difference between these cumulative probabilities and their limits. Finally, we will calculate P_{12} on M and $\bar{M}$.

4.1.5.2 *Convergence to 0 of the cumulative probability that $(\hat{t}_1, \hat{t}_2)$ is in $\bar{M}$.* To enable the proof that the cumulative probability of $(\hat{t}_1, \hat{t}_2)$ being in $\bar{M}$ converges to 0 monotonically as SN_1 and SN_2 increase without bound, we define

$$\delta = \iint_{\bar{M}} P_{12}(v_1, v_2 | x_c, t_{0c})\, dv_1 dv_2 \,. \tag{44}$$

Since the entire t_1, t_2 plane comprises M and $\bar{M}$ and since the cumulative probability that $-\infty < \hat{t}_1 < \infty$ and $-\infty < \hat{t}_2 < \infty$ is 1, δ can be calculated from

$$\delta = 1 - \iint_{M} P_{12}(v_1, v_2\, x_c, t_{0c})\, dv_1 dv_2 \,. \tag{45}$$

Since $F_{12} = F$ and since $F(t_1, t_2 | x_c, t_{0c}) = 0$ for $t_1 < t_{p1}$ or $t_2 < t_{p2}$, we obtain from Eq. (45)

$$\delta = 1 - F(t_1, t_2 | x_c, t_{0c}) \,. \tag{46}$$

Then, since $F_l \leq F$, we have, after combining Eqs. (19), (39), and (46),

$$\delta \leq 1 - F_l(t_{v1}, t_{v2} | x_c, t_{0c}) = D \,. \tag{47}$$

where

$$D = C + L \tag{48}$$

and

$$L = 1 - \int_{t_{p2}}^{t_{v2}} \int_{t_{p1}}^{t_{v1}} H(v_1, v_2 | x_c, t_{0c})\, dv_1 dv_2 \,. \tag{49}$$

Since $r_1(t)$ and $r_2(t)$ are absolutely continuous [27] and monotonic in M, each of the iterated single integrals in Eq. (49) may be interpreted as a Stieltjes integral [32]. By using this interpretation, together with Eqs. (41), (47), (48), and (49),

$$\bar{\delta} \leq 1 + 0.25[\operatorname{erfc}\beta_{p1}\operatorname{erfc}\beta_{v2} + \operatorname{erfc}\beta_{p2}\operatorname{erfc}\beta_{v1} - \operatorname{erfc}\beta_{v1}\operatorname{erfc}\beta_{v2}] \,. \tag{50}$$

where

$$\beta_{p1} = r_1(t_{p1})(2k_{11})^{-1/2} \,,$$

$$\beta_{v1} = r_1(t_{v1})(2k_{11})^{-1/2} \,,$$

$$\beta_{p2} = r_2(t_{p2})(2k_{22})^{-1/2} \,,$$

and

$$\beta_{v2} = r_2(t_{v2})(2k_{22})^{-1/2} \,.$$

is obtained. Equation (50), when coupled with the definitions given by Eqs. (42) and (43), proves that $\bar{\delta}$ converges monotonically to 0 as SN_1 and SN_2 increase without bound.

4.1.5.3 *Convergence of F to F_l on M as SN_1 and SN_2 increase without bound.* To enable the proof that F converges monotonically and uniformly to F_l on M as SN_1 and SN_2 increase without bound, $\delta(t_1, t_2)$ is defined by

$$\delta(t_1, t_2) = F(t_1, t_2 | x_c, t_{0c}) - F_l(t_1, t_2 | x_c, t_{0c}) \,. \tag{51}$$

Then, we observe that

$$\begin{aligned} \delta(t_1, t_2) &\leq F_u(t_1, t_2 | x_c, t_{0c}) - F_l(t_1, t_2 | x_c, t_{0c}) \\ &= C + G(t_1, t_2) \,, \end{aligned} \tag{52}$$

where

$$G(t_1, t_2) = \int_{t_{p2}}^{t_2} \int_{t_{p1}}^{t_1} E(v_1, v_2)\, dv_1 dv_2 \,.$$

$$E(t_1, t_2) = E_1(t_1, t_2) E_2(t_1, t_2) ,$$

$$E_1(t_1, t_2) = K \exp\{[-u_3(t_1) - u_4(t_2)]/2\} ,$$

$$E_2(t_1, t_2) = y_1(t_1) y_2(t_2) \{G[-y_1(t_1)] G[-y_2(t_2)] - 1\} ,$$

and

$$K = \pi^{-1}(k_{33}/k_{11})^{1/2}(k_{44}/k_{22})^{1/2} .$$

The intermediate variables of Eq. (52) [namely, $y_1(t_1)$, $y_2(t_2)$, $u_3(t_1)$, and $u_4(t_2)$], as well as the function $G(y)$ are defined in Eq. (36). Then, since y_1 and y_2 are negative on M,

$$E_2(t_1, t_2) < \exp[-y_1^2(t_1) - y_2^2(t_2)]$$
$$- 0.5\pi^{-1/2}\{y_1(t_1)\exp[-y_2^2(t_2)] + y_2(t_2)\exp[-y_1^2(t_1)]\} \quad (53)$$

is obtained. By using Eqs. (12) and (13) and the definitions of k_{ij}, which are given in conjunction with Eq. (31), all of the intermediate variables in Eqs. (52) and (53) can be rewritten as the product of appropriate signal-to-noise ratios and normalized response functions. However, we will omit the details of such rewriting and point out that, after such rewriting, the limit of $E(t_1, t_2)$ as SN_1 and SN_2 increase without bound is the same as the limit, before rewriting, of $E(t_1, t_2)$ as u_3, u_4, y_1, and y_2 increase without bound. Furthermore, we point out that, after such rewriting, K is not a function of SN_1 or SN_2. Therefore, according to Eqs. (52) and (53), if $\dot{r}_1(t_{c1}) \neq 0$ and $\dot{r}_2(t_{c2}) \neq 0$, and $r_1(t)$ and $r_2(t)$ are continuous on M, then $E(t_1, t_2)$ converges monotonically and uniformly to 0 on M as SN_1 and SN_2 increase without bound. Then, since the measure of M is finite, $G(t_1, t_2)$ converges monotonically and uniformly to 0 on M as SN_1 and SN_2 increase without bound. Finally, since Eq. (41) shows that C converges monotonically to 0 as SN_1 and SN_2 increase without bound, it is clear that $\delta(t_1, t_2)$ converges monotonically and uniformly to 0 on M as SN_1 and SN_2 increase without bound.

4.1.5.4 *Effects of finite values of SN_1 and SN_2 on $\bar{\delta}$ and δ.* The effects of finite SN_1 and SN_2 on $\bar{\delta}$ can be calculated from Eq. (50). For $r_1(t_{v1}) \approx -r_1(t_{p1})$, $r_2(t_{v2}) \approx -r_2(t_{p2})$, $SN_1 \geq 10$, and $SN_2 \geq 10$, $\bar{\delta}$ is less than 10^{-22}. This upper bound for $\bar{\delta}$, which is the total probability of the pair of random variables $(\hat{t}_1, \hat{t}_2)$ being in $\bar{M}$, is small enough compared with 1 that, after noting that P_{12} is nowhere negative, we conclude that

$$P_{12} = 0 \quad (54)$$

on $\bar{M}$ if $SN_1 \geq 10$ and $SN_2 \geq 10$.

Unfortunately, we have not been able to formulate an expression for δ that does not require numerical integration to implement it when SN_1 and SN_2 are finite. However, because of the monotonic convergence of δ to 0 as SN_1 and SN_2 increase without bound, a numerical calculation of the maximum value of δ on M for particular pulse shapes, $r_1(t)$ and $r_2(t)$, and particular values of SN_1 and SN_2 establishes for these pulse shapes an upper bound for the maximum value of δ on M for all greater values of SN_1 and SN_2. For these reasons, we have used numerical integration of $E(t_1, t_2)$ as indicated by Eq. (52), combined with the straightforward calculation of C, to calculate $\delta(t_1, t_2)$ on M for representative pulse shapes. From the results of these calculations, we conclude that

$$\delta(t_1, t_2) < 10^{-23}(t_1 - t_{p1})(t_2 - t_{p2})(t_{v1} - t_{p1})^{-1}(t_{v2} - t_{p2})^{-1} \tag{55}$$

on M if $SN_1 > 10$ and $SN_2 > 10$. Since the maximum value of δ on M for representative pulse shapes is, according to Eq. (55), negligible compared with values of F near its mean (where F is of the order of 0.25), we conclude that

$$F = F_l \tag{56}$$

on M if $SN_1 > 10$ and $SN_2 > 10$.

4.1.5.5 *Specification of $P_{12}(t_1, t_2|x_c, t_{0c})$ for $SN_1 > 10$ and $SN_2 > 10$.* By combining Eqs. (19), (39), (41), (54), and (56), we find that for $SN_1 > 10$ and $SN_2 > 10$ the joint probability density function P_{12} is given by

$$P_{12}(t_1, t_2|x_c, t_{0c}) = M(t_1, t_2)\, U(t_1 - t_{p1})\, U(t_{v1} - t_1)\, U(t_2 - t_{p2})\, U(t_{v2} - t_2), \tag{57}$$

where $U(z)$ is the unit step function and $M(t_1, t_2)$ is defined in connection with Eq. (36). The requirement that SN_1 and SN_2 be greater than 10 is not restrictive for our application because the signal-to-noise ratios of typical operating PSDs are greater than 100 [33].

4.2 Marginal Density Function $P_3(t_3|x_c)$

4.2.1 **Derivation of $P_3(t_3|x_c)$ from $P_{12}(t_1, t_2|x_c, t_{0c})$.** To obtain $P_3(t_3|x_c)$ from $P_{12}(t_1, t_2|x_c, t_{0c})$, first $P_{13}(t_1, t_3|x_c, t_{0c})$ is obtained by implementing the transformation

$$t_1 = t_1 ,$$

$$t_3 = t_2 - t_1 .$$

Since the Jacobian of this transformation is 1, the result of this implementation is

$$P_{13}(t_1, t_3|x_c, t_{0c}) = M(t_1, t_1 + t_3)\, U(t_3 - t_{l3})\, U(t_{u3} - t_3)\, U(t_1 - t_{l1})\, U(t_{u1} - t_1), \tag{58}$$

where

$$t_{l3} = t_{p2} - t_{v1} ,$$

$$t_{u3} = t_{v2} - t_{p1} ,$$

$$t_{l1} = (t_{p2} - t_3)\, U(t_{p2} - t_{p1} - t_3) + t_{p1}\, U(t_3 - t_{p2} + t_{p1}) ,$$

$$t_{u1} = (t_{v2} - t_3)\, U(t_3 - t_{v2} + t_{v1}) + t_{v1}\, U(t_{v2} - t_{v1} - t_3) .$$

The region in the t_1, t_3 plane within the boundaries defined by the unit step functions of Eq. (58) is called O. The region O is the image of the region M.

Next, P_3 is obtained from P_{13} by calculating the marginal density function

$$P_3(t_3|x_c) = \int_{-\infty}^{\infty} P_{1,3}(t_1, t_3|x_c, t_{0c})\,dt_1 \; . \quad (59)$$

To implement Eq. (59), approximations for $r_1(t)$ and $r_2(t)$ are usually necessary. We believe the use of linear approximations effects the best compromise between accuracy of results and complexity of derivations. The linear approximations that we use are

$$r_1(x_c, t) = (t - t_{c1})S_{t1} \; , \quad (60)$$

$$r_2(x_c, t) = (t - t_{c2})S_{t2} \; , \quad (61)$$

where

$$S_{t1} = [\partial r_1(x_c, t)/\partial t]_{t = t_{c1}}$$

and

$$S_{t2} = [\partial r_2(x_c, t)/\partial t]_{t = t_{c2}} \; .$$

The pulse epoch, t_{0c}, may be taken as 0 when calculating S_{t1} and S_{t2}. By using Eqs. (58), (60), and (61) and the definition of W from Eq. (36) in Eq. (59), P_3 is determined to be [34]

$$P_3(t_3|x_c) = 0.5(2\pi)^{-1/2}\sigma_3^{-1}\, C(t_{l1}, t_{u1}, t_3')\, S(t_3') \exp(-t_3'^2/2\sigma_3^2) \; , \quad (62)$$

where

$$t_3' = t_3 - \bar{t}_3 \; ,$$

$$\bar{t}_3 = t_{c2} - t_{c1} \; ,$$

$$\sigma_3^2 = \sigma_1^2 + \sigma_2^2 \; ,$$

$$\sigma_1^2 = k_{11}/S_{t1}^2 \; ,$$

$$\sigma_2^2 = k_{22}/S_{t2}^2 \; ,$$

$$C(t_{l1}, t_{u1}, t_3') = \mathrm{erf}[Z(t_{u1}, t_3')] - \mathrm{erf}[Z(t_{l1}, t_3')] \; ,$$

$$Z(t, t_3') = 2^{-1/2}\sigma_2^{-1}[(t - t_{c1})\sigma_3\sigma_1^{-1} + \sigma_1\sigma_3^{-1}t_3'] \; ,$$

$$S(t_3') = U(t_3' - t_l')\,U(t_u' - t_3') \; ,$$

$$t_l' = (t_{p2} - t_{c2}) + (t_{c1} - t_{v1}) \; ,$$

$$t_u' = (t_{v2} - t_{c2}) + (t_{c1} - t_{p1}) \; .$$

As expected, P_3 is completely independent of pulse epoch, t_{0c}.

4.2.2 Effect on P_3 of the use of linear approximations for $r(t)$. Some error is introduced into Eq. (59) as a result of using linear approximations for $r_1(t)$ and $r_2(t)$ in the region M. However, this error converges monotonically and uniformly to 0 on M as SN_1 and SN_2 increase without bound. This convergence occurs because $r^2(t)$ appears in the equation for P_3 as a negative exponent of e.

To determine the magnitude of this error for finite SN_1 and SN_2, we have selected typical response functions $r_1(t)$ and $r_2(t)$ and used numerical integration of P_{13}, as indicated by Eq. (59), to calculate P_3 for various SN_1 and SN_2. We compared these results with corresponding calculations of P_3 according to Eq. (62) for Gaussian-shaped pulses. For $SN_1 = 20$, $SN_2 = 20$, and any t_3, the difference between these two calculated values of P_3 is typically less than $1.5 \times 10^{-3} P_3(t_3|x_c)$. Hence, we conclude that Eq. (62) is more than adequate to predict the performance of operating PSDs, for which SN_1 and SN_2 are typically much greater than 20. However, for particular PSDs for which there is doubt as to the validity of the linear approximations for $r(t)$, numerical integration can be used instead.

4.2.3 Approximation of P_3 with a normal probability density function. Equation (62) can be simplified to that for a normal probability density function with negligible change in the values of P_3. To make this simplification, $C(t_{l1}, t_{u1}, t_3')$ is replaced with 2, and the switching function $S(t_3')$ is replaced with 1.

We first consider the effect of replacing $C(t_{l1}, t_{u1}, t_3')$ with 2. For any t_3' in O, $C(t_{l1}, t_{u1}, t_3')$ converges uniformly and monotonically to 2 as SN_1 and SN_2 increase without bound. Furthermore, for $SN_1 = SN_2 = 20$, $\sigma_1 = \sigma_2$, $r_1(t_{p1}) \approx -r_1(t_{v1})$, $r_2(t_{p2}) \approx -r_2(t_{v2})$, and $|t_3'/\sigma_3| \leq 20$, the difference $2 - C(t_{l1}, t_{u1}, t_3')$ is less than 10^{-15}. Proofs of these statements are facilitated by noting that $\sigma_1 SN_1 \approx t_{c1} - t_{p1}$ and $\sigma_2 SN_2 \approx t_{c2} - t_{p1}$. Since the difference $2 - C(t_{l1}, t_{u1}, t_3')$ is small and since the requirement $|t_3'/\sigma_3| \leq 20$ excludes very little of the P_3 distribution, we consider P_3 adequately represented by a normal density function with standard deviation σ_3 and mean t_3, truncated according to $S(t_3')$.

We next consider the effect of untruncating the P_3 density function. Since $t_u' \approx \sigma_2 SN_2 + \sigma_1 SN_1$ and $t_l' \approx -t_u'$, the effect of the switching function $S(t_3')$ for $SN_1 \geq 20$ and $SN_2 \geq 20$ is to cause the truncated normal density function to be 0 for values of t_3' where the values of the untruncated normal density function are less than 10^{-178} times the maximum value of P_3. Hence, we simplify Eq. (62) by replacing $S(t_3')$ with 1. With this simplification, P_3 is given by

$$P_3(t_3|x_c) = (2\pi)^{-1/2} \sigma_3^{-1} \exp(-t_3'^2/2\sigma_3^2) \tag{63}$$

for SN_1 and SN_2 greater than 20. The probability density function $P_3(t_3|x_c)$ characterizes the output variable from the time analyzer in Fig. 1. We next consider the transformation of this probability density function to that for the random variable $\hat{x}_c$.

4.3 Asymptotic Approximation to the Decoder Density Function

4.3.1 Derivation of $P_d(x_c|x_c)$ from $P_3(t_3|x_c)$. The decoding equation $t_3(x_c)$, which is needed to transform $P_3(t_3|x_c)$ into an asymptotic approximation to the decoder density function, is implicitly defined by the system of equations

$$
\begin{aligned}
&r_1(x_c, t_1) = 0\,, \\
&r_2(x_c, t_2) = 0\,, \\
&t_3 = t_2 - t_1\,.
\end{aligned} \tag{64}
$$

To approximate the function $t_3(x_e)$ implied by Eq. (64), we use one two-variable linear Taylor series expansion to approximate $r_1(x_e, t_1)$, and we use a second one to approximate $r_2(x_e, t_2)$. These Taylor series are

$$r_1(x_e, t_1) = (x_e - x_c)S_{x1} + (t_1 - t_{c1})S_{t1}$$

and

$$r_2(x_e, t_2) = (x_e - x_c)S_{x2} + (t_2 - t_{c2})S_{t2} , \tag{65}$$

where

$$S_{x1} = [\partial r_1(x, t)/\partial x]_{t = t_{c1},\, x = x_c}$$

and

$$S_{x2} = [\partial r_2(x, t)/\partial x]_{t = t_{c2},\, x = x_c} .$$

Again, the pulse epoch may be taken as zero to calculate S_{t1}, S_{t2}, S_{x1}, and S_{x2}. In addition, although we have not indicated it explicitly, all of these parameters are functions of $a_1, \ldots, a_n$ as well as of x_c.

Then, Eqs. (64) and (65) are used together to yield

$$t_3'(x_e) = t_3(x_e) - t_3 = (x_e - x_c)S , \tag{66}$$

where

$$S = S_{x1}S_{t1}^{-1} - S_{x2}S_{t2}^{-1} .$$

By using Eq. (66) together with Eq. (63), we finally obtain

$$P_d(x_e|x_c) = (2\pi)^{-1/2}\sigma_x^{-1} \exp[-(x_e - x_c)^2/2\sigma_x^2] \approx P_d(x_e|x_c) , \tag{67}$$

where

$$\sigma_x^2 = \sigma_3^2/S^2 .$$

Because of the approximations we have used in the derivation of $P_d(x_e|x_c)$, we explicitly indicate that it is only approximately equal to $P_d(x_e|x_c)$.

If $x_c = L/2$ and the encoder is operated in the balanced mode (i.e., except for extra delay in channel 2 to make the stop pulse always arrive after the start pulse, channel 1 and channel 2 are identical), then $S_{x1} = -S_{x2}$, and the equation for σ_x reduces to

$$\sigma_x^2 = k_{11}/(2S_{x1}^2) = k_{22}/(2S_{x2}^2) . \tag{68}$$

4.3.2 Effect on $P_d(x_e|x_c)$ of the use of linear approximations for $r(x, t)$. For any given exact $t_3(x_e)$ and for a given nonzero S, the error in $P_d(x_e|x_c)$ caused by the use of Eq. (66) converges monotonically and uniformly to 0 for $0 \leq x_e \leq L$ as SN_1 and SN_2 increase without bound. Before this error can be characterized further, the encoder modulation characteristics $[v_1(x_c, t_{0c}, t)$ and $v_2(x_c, t_{0c}, t)]$ and the impulse responses $[h_1(t)$ and $h_2(t)]$ of the filters must be specified. Then, numerical methods can be used to calculate the exact $t_3'(x_e)$ and the error in P_a that is caused by the use of linear approximations. For an optimized PSD that uses an RC position-sensitive proportional counter [1] with $SN_1 = SN_2 = 20$, we find this error to be less than 4×10^{-4} $P_a(x_e|x_c)$ for $x_c = L/2$ and $0 \leq x_e \leq L$. Hence we conclude that the effect on P_a of this approximation is negligible for signal-to-noise ratios greater than 20.

4.3.3 **Convergence of $P_a(x_e|x_c)$ to $P_d(x_e|x_c)$.** Because, as we have pointed out at the appropriate places in this work, the separate errors caused by our various approximations converge monotonically to zero, the total-error function $E_T(x_e, x_c)$, where

$$E_T(x_e, x_c) = P_a(x_e|x_c) - P_d(x_e|x_c),$$

converges monotonically to zero with increasing SN_1 and SN_2 for all x_e and x_c and for all r_1 and r_2. Furthermore, our numerical calculations of E_T for Gaussian-derivative-shaped r_1 and r_2 indicate that, for $SN_1 = SN_2 = 20$,

$$|E_T(x_e, x_c)| \leq 2 \times 10^{-3} P_m,$$

where P_m is the maximum value of P_d. In addition, $E_T(x_e, x_c)$ typically changes sign, so that σ_x as given by Eq. (67) differs from the numerically calculated square root of the second moment of P_d about its mean by less than 0.5% for $SN_1 = SN_2 = 20$. For these reasons, we believe Eq. (67) is, when used with Eq. (2), more than adequate to predict the performance of and to derive the optimum position decoding filters for operating detectors, where SN_1 and SN_2 are typically greater than 20.

5. APPLICATIONS

The starting point for the computation of the overall PSF for a PSD is specification of the functional forms of the photon-caused pulses $v_1(x_c, a_1, \ldots, a_n, t_{0c}, t)$ and $v_2(x_c, a_1, \ldots, a_n, t_{0c}, t)$ and the noise autovariance functions $\Gamma_{11}(\tau)$ and $\Gamma_{22}(\tau)$. The functions v_1 and v_2 are most easily determined by calculations based on a model of the particular position encoder being used. However, the autovariance functions Γ_{11} and Γ_{22} can be determined either from theoretical calculations or from Fourier transform inverses of experimentally determined noise power spectral densities.

Although we have assumed for purposes of illustration that these functions are specified at the outputs of the position encoder, there is no change in the computation method for specification of v_1 and Γ_{11} at one arbitrarily chosen point p_1 in the chain of amplifiers and filters that comprise channel 1 and the specification of v_2 and Γ_{22} at another arbitrarily chosen point p_2 in the chain of amplifiers and filters that comprise channel 2. For any p_1, $h_1(t)$ is the impulse response of the portion of channel 1 between p_1 and the crossover detector D_1. Similarily, for any p_2, $h_2(t)$ is the impulse response of the portion of channel 2 between p_2 and the crossover detector D_2. For analysis of a PSD, the points p_1 and p_2 can be chosen so that h_1 and h_2 are delta functions. For determination of optimum filters, p_1 and p_2 are chosen so that the noise at each point is white.

Next, k_{11} and k_{22} are computed from Γ_{11}, Γ_{22}, h_1, and h_2 by using Eqs. (12) and (13) and the definitions associated with Eq. (31). The response functions $r_1(x_c, a_1, \ldots, a_n, t_{0c}, t)$ and $r_2(x_c, a_1, \ldots, a_n, t_{0c}, t)$ are calculated from v_1, v_2, h_1, and h_2 by using Eqs. (8) and (9). For typical operating PSDs, for which the signal-to-noise ratios are greater than 100, the various approximations we have used are completely justified. For these PSDs. the various parameters of $P_d(x_e|x_c, a_1, \ldots, a_n)$, particularly σ_x, are calculated from k_{11}, k_{22}, r_1, and r_2 and the definitions of Eqs. (61), (62), (65), and (67). However, for PSDs with signal-to-noise ratios less than 20, the validity of the various approximations should be investigated by numerical techniques as we have indicated. For PSDs for which electronic noise is the dominant reason that P is not a delta function, $P_d(x_e|x_c)$ is the overall PSF. For other PSDs, the overall PSF $P(x_e|v_0)$ is calculated from $P_d(x_e|x_c, a_1, \ldots, a_n)$ and the encoder density function $P_e(x_c, a_1, \ldots, a_n|v_0)$, which must be specified according to the dominant statistical processes in the particular encoder being used, according to Eq. (2).

ACKNOWLEDGMENTS

We thank C. J. Borkowski for his patient support and encouragement; T. V. Blalock, M. K. Kopp, and F. H. Clark for many stimulating and helpful discussions; and J. L. Blankenship for his critical review.

REFERENCES

1. C. J. Borkowski and M. K. Kopp, "New Type of Position-Sensitive Detectors of Ionizing Radiation Using Risetime Measurement," *Rev. Sci. Instrum.* **39**, 1515–22 (October 1968).

2. C. J. Borkowski and M. K. Kopp, "Some Applications and Properties of One- and Two-Dimensional Position-Sensitive Proportional Counters," *IEEE Trans. Nucl. Sci.* **NS-17**, 340–49 (June 1970).

3. C. J. Borkowski and M. K. Kopp, "Proportional Counter Photon Camera," *IEEE Trans. Nucl. Sci.* **NS-19**, 161–68 (June 1972).

4. A. W. Stetz, V. Perez-Mendez, J. Geaga, and H. Spinka, "Characteristics of Multiwire Proportional Counters with Delay-Line Readout for Minimum-Ionizing Particles," *Nucl. Instrum. Methods* **120**, 17–22 (Aug. 15, 1974).

5. R. Grove, I. Ko, B. Leskovar, and V. Perez-Mendez, "Phase Compensated Electromagnetic Delay Lines for Wire Chamber Readout," *Nucl. Instrum. Methods* **99**, 381–85 (Mar. 1, 1972).

6. J. Hough, "An Investigation of Some Fundamental Limitations to the Spatial Resolution of a Gas Proportional Counter," *Nucl. Instrum. Methods* **105**, 323–28 (Dec. 1, 1972).

7. E. Mathieson, "Linearity and Noise Considerations for Position Sensitive Detectors," *Nucl. Instrum. Methods* **97**, 171–76 (Nov. 15, 1971).

8. V. Radeka, "Signals, Noise and Resolution in Position-Sensitive Detectors," *IEEE Trans. Nucl. Sci.* **NS-21**, 51–64 (February 1974).

9. I. F. Blake and W. C. Lindsey, "Level-Crossing Problems for Random Processes," *IEEE Trans. Inf Theory* **IT-19**, 295–315 (May 1973).

10. H. Cramer, *Mathematical Methods of Statistics*, Princeton, N.J.: Princeton University Press, 1951, pp. 268–69.

11. A. Papoulis, *Probability, Random Variables and Stochastic Processes*, New York: McGraw-Hill, 1965, pp. 233–37.

12. *See ref. 11, p.* 88.

13. E. L. O'Neill, *Introduction to Statistical Optics*, Reading, Mass.: Addison-Wesley Publishing Co., 1963.

14. D. J. Stigliani, R. Mittka, and R. G. Semonin, "Resolving Power of a Zone Plate," *J. Opt. Soc. Am.* **57**, 610–13 (May 1967).

15. D. Middleton, *Introduction to Statistical Communication Theory*, New York: McGraw-Hill, 1960, p. 27.

16. See ref. 15, chap. 11.

17. See ref. 15, chaps. 7 and 8.

18. See ref. 15, p. 53.

19. See ref. 15, p. 171.

20. See ref. 11, pp. 345–46.

21. See ref. 15, p. 189.

22. See ref. 11, pp. 352–53.

23. S. O. Rice, "Mathematical Analysis of Random Noise," *Bell Syst. Tech. J.*, 24, 46–156 (January 1945).

24. D. J. Torrieri, "The Uncertainty of Pulse Position Due to Noise," AD-745 294, Naval Research Laboratory, Washington, D.C., May 31, 1972.

25. M. R. Leadbetter, "On Crossings of Levels and Curves by a Wide Class of Stochastic Processes," *Ann. Math. Stat.* 37, 260–67 (1966).

26. H. Cramer and M. R. Leadbetter, *Stationary and Related Stochastic Processes*, New York: John Wiley & Sons, Inc., 1967, pp. 283–91.

27. M. J. Lighthill, *Fourier Analysis and Generalized Functions*, New York: Cambridge University Press, 1964.

28. See ref. 10, pp. 166–72 and 260–63.

29. See ref. 15, p. 350.

30. See ref. 15, p. 153.

31. See ref. 15, p. 1079.

32. S. Hartman and J. Mikusinski, *The Theory of Lebesgue Measure and Integration*, New York: Pergamon Press, 1961, chap. 13.

33. C. J. Borkowski, M. K. Kopp, and J. A. Harter, "Line-Scanning Proportional Counter Camera," *IEEE Trans. Nucl. Sci.* NS-22(2), 896–900 (April 1975).

34. M. Abramowitz and I. A. Stegun, eds., *Handbook of Mathematical Functions* (Applied Mathematics Series 55), Washington, D.C.: NBS, 1964, p. 303 Eq. 7.4.32.

ORNL-5081
UC-32 -- Mathematics and Computers

INTERNAL DISTRIBUTION

1. C. J. Borkowski
2. F. L. Culler
3. R. F. Hibbs
4-33. C. H. Nowlin
34. H. Postma
35. C. R. Richmond
36. P. H. Stelson
37-38. Central Research Library
39. Document Reference Section
40-42. Laboratory Records Department
43. Laboratory Records, ORNL R.C.
44. ORNL Patent Office

EXTERNAL DISTRIBUTION

45-46. Director, Division of Biomedical and Environmental Research, Energy Research and Development Administration, Washington, DC 20545
47. Director, Research and Technical Support Div. ERDA-ORO
48. Prof. I. F. Blake, Department of Electrical Engineering, University of Waterloo, Waterloo, Ontario D0650
49. Prof. C. W. Helstrom, Department of Applied Physics and Information Science, University of California, La Jolla, CA 92037
50. Prof. M. Kac, Department of Mathematics, Rockefeller University, New York, NY 10021
51. Prof. M. R. Leadbetter, Department of Statistics, University of North Carolina, Chapel Hill, NC 27514
52. Prof. W. C. Lindsey, Department of Electrical Engineering, University of Southern California, University Park, Los Angeles, CA 90007
53. Prof. D. Middleton, Department of Electrical Engineering, University of Rhode Island, Kingston, RI 02881
54. David Middleton, 127 E. 91st Street, New York, NY 10028
55. Prof. A. Papoulis, Department of Electrical Engineering, Polytech Institute, Brooklyn, NY 11201
56. Prof. A. J. F. Siegert, Department of Physics, Northwestern University, Evanston, IL 60201
57. Prof. D. Slepian, Department of Electrical Engineering, University of Hawaii at Manoai, Honolulu, HI 96822
58. Mr. H. R. Wasson, Environmental and Biomedical Research, Energy Research and Development Administration, Washington, DC 20545
59. Dr. D. A. Mack, Lawrence Radiation Laboratory, The University of California, Berkeley, CA 94720
60. Dr. G. L. Miller, Bell Labs, Murray Hill, NJ 07974
61. Dr. E. Gatti, C.I.S.E., Via Procaccini, N. 1, Milano, Italy

62. Dr. F. S. Goulding, Lawrence Radiation Laboratory, University of California, Berkeley, CA 94720
63. Dr. E. H. Cooke-Yarborough, Head, Electronics and Applied Physics Division, Atomic Energy Research Establishment, Harwell, Didcot, Berks, England
64. E. Mathieson, Physics Department, University of Leicester, Leicester LE1 7RH, England
65. Dr. Henry M. Paynter, Department of Mechanical Engineering, Massachusetts Institute of Technology, Cambridge, MA 02139
66. Dr. Joseph Anthony Thie, P.O. Box 517, Barrington, IL 60010
67. Dr. Lawrence G. Rubin, National Magnet Laboratory, Massachusetts Institute of Technology, 170 Albany Street, Cambridge, MA 02139
68. Dr. Klaus-Dieter Muller, Zentrallabor fur Elektronik/Nukleare Elektronik, 517 Julich Privat, Postfach 365, Mannheimer StraBe 2, Germany
69. Dr. M. G. Strauss, Argonne National Laboratory, 9700 S. Cass Avenue, Argonne, IL 30439
70. Dr. J. Schelten, Institut fur Festkorperforschung, Kernforschungsanlage Julich, 517 Julich, Germany
71. Dr. V. Radeka, Brookhaven National Laboratory, Upton, Long Island, NY 11973
72. C. R. Fisher, ERDA, Federal Office Building, Oak Ridge, TN 37830
73. Library, Battelle Memorial Institute, Columbus Laboratories, 505 King Avenue, Columbus, OH 43201
74. Library, Bolt Beranek and Newman Inc., 50 Moulton Street, Cambridge, MA 02138
75. Library, Brigham Young University, Provo, UT 84601
76. Physical Sciences Library, Brown University, Providence, RI 02912
77. Library, Division of Geological Sciences, California Institute of Technology, Pasadena, CA 91109
78. Mathematics and Science Library, Columbia University, 303 Mathematics Building, New York, NY 10027
79. Physical Sciences Library, Clark Hall, Cornell University, Ithaca, NY 14850
80. School of Engineering Library, Duke University, Durham, NC 27706
81. Anna Aghamianz, Technical Reports Collection, Gordon McKay Library, Harvard University, Pierce Hall 305, 29 Oxford Street, Cambridge, MA 02138
82. Prof. N. Donald Ylvisaker, Department of Mathematics, University of California, Los Angeles, CA 90024
83. Dr. S. O. Rice, Bell Telephone Laboratories, Mountain Ave, Murray Hill, NJ 07974
84. Harvey M. Phillips, Ruddock House 1-55 CalTech, Pasadena, CA 91126
85. Dr. Ronald Nutt, ORTEC, Oak Ridge, TN 37830
86. Dr. V. Perez-Mendez, Lawrence Radiation Laboratory, University of California, Berkeley, CA 94720
87. Neven Karlovac, ORTEC, Oak Ridge, TN 37830
88. Widner Library, Harvard University, Cambridge, MA 02138
89. Don J. Torrieri, Naval Research Laboratory, 4555 Overlook Ave., S.W., Washington, DC 20390
90. Library, Astronomy-Physics-Mathematics, Swain Hall, Indiana University, Bloomington, IN 47401
91. Library, Indiana University of Pennsylvania, Indiana, PA 15701
92. Library, Engineering Research Institute, Iowa State University of Science and Technology, Ames, IA 50010
93. University Library, Kent State University, Kent, OH 44240
94. Library, Center for Marine and Environmental Studies, Lehigh University, Bethelehem, PA 18015
95. Library, Naval Research Laboratory, 4555 Overlook Avenue, S.W., Washington, DC 20390
96. Library, Department of Experimental Statistics, North Carolina State University, Box 5457, Raleigh, NC 27607
97. Library, College of Engineering, Northeastern University, 360 Huntington Avenue, Boston, MA 02115

98. Mathematics Library, Lunt Hall Room 11, Northwestern University, Evanston, IL 60201
99. Engineering Library, Ohio State University, 2024 Neil Avenue, Columbus, OH 43210
100. Berks Center Library, Pennsylvania State University, 108 North 8th Avenue, Wyomissing, PA 19610
101. Director of Libraries, Polytechnic Institute of Brooklyn, 333 Jay Street, Brooklyn, NY 11201
102. Engineering Library, School of Engineering and Applied Science, Princeton University, Princeton, NJ 08540
103. Technical Information Service, Main Library, Room 200A, Stanford University, Stanford, CA 94305
104. Electro-Optical Sciences Center, c/o Professor George W. Stroke, Department of Electrical Sciences, State University of New York, Stony Brook, NY 11790
105. Lufkin Engineering Library, Anderson Hall, Tufts University, Medford, MA 02155
106. Engineering Library, University of Alabama, P.O. Box 6267, University, AL 35486
107. Science Division Library, University of Arizona, Tucson, AZ 85721
108. Library, Graduate Institute of Technology, University of Arkansas, P.O. Box 3017, Little Rock, AR 72203
109. General Library, University of California, Berkeley, CA 94720
110. Library, Engineering and Mathematical Sciences, University of California, 405 Hilgard Avenue, Los Angeles, CA 90024
111. Library, Division of Physical Sciences, University of Chicago, 1118 East 58th Street, Chicago, IL 60637
112. Science and Technology Libraries, University of Colorado, Boulder, CO 80302
113. Library, Department of Physics and Astronomy, University of Florida, Gainesville, FL 32601
114. General Research Library, University of Georgia, Athens, GA 30601
115. Science-Technology Library, University of Hawaii, Honolulu, HI 96822
116. Library, College of Engineering, University of Illinois, 112 Engineering Hall, Urbana, IL 61801
117. Engineering Library, University of Kentucky, Lexington, KY 40506
118. Library, Institute for Fluid Dynamics and Applied Mathematics, University of Maryland, College Park, MD 20742
119. School of Engineering Library, University of Massachusetts, Amherst, MA 01002
120. Mathematics Library, 3027 Angell Hall, University of Michigan, Ann Arbor, MI 48104
121. Library, University of Minnesota, Minneapolis, MN 55455
122. Library, University of Missouri, Rolla, MO 65401
123. Mathematics-Physics Library, University of North Carolina, Phillips Hall, Chapel Hill, NC 27514
124. College of Engineering Library, University of Notre Dame, Notre Dame, IN 46556
125. Mathematics-Physics Library, University of Pennsylvania, 209 South 33d Street, Philadelphia, PA 19104
126. Library, Division of Engineering Research and Development, University of Rhode Island, Bliss Hall, Kingston, RI 02881
127. Engineering Library, Ferris Hall, University of Tennessee, Knoxville, TN 37916
128. Dr. T. V. Blalock, Electrical Engineering Department, Ferris Hall, University of Tennessee, Knoxville, TN 37916
129. Library, Applied Research Laboratories, The University of Texas, P.O. Box 8029, Austin, TX 78712
130. University of Toledo Library, 2801 West Bancroft Street, Toledo, OH 43606
131. Library, School of Engineering and Applied Science, University of Virginia, Thornton Hall, Charlottesville, VA 22901
132. Library, Science/Technology Information Center, University of Virginia Library, Charlottesville, VA 22901
133. Library, University of Washington, Seattle, WA 98105
134. Mathematics Research Center, U.S. Army, University of Wisconsin, Madison, WI 53706
135. Physics-Mathematics Library, Van Vleck Hall, University of Wisconsin, Madison, WI 53706
136. Carol M. Newman Library, Virginia Polytechnic Institute and State University, Blacksburg, VA 24061

137. General Library, West Virginia University, Morgantown, WV 26506
138. George C. Gordon Library, Worcester Polytechnic Institute, Worcester, MA 01609
139. Engineering and Applied Science Library, Yale University, 15 Prospect Street, New Haven, CT 06520
140. Sciences and Engineering Library, University of California San Diego, La Jolla, CA 92037
141. Sciences and Engineering Library, University of California at Irvine, Irvine, CA 92664
142. Sciences and Engineering Library, California State University, 1600 Holloway Avenue, San Francisco, CA 94132
143. Science and Engineering Library, California State University Sacramento, 6000 Jay Street, Sacramento, CA 95819
144. Sciences and Engineering Library, University of Iowa, Iowa City, IA 52240
145. Sciences and Engineering Library, Kansas State University, Manhattan, KS 66506
146. Sciences and Engineering Library, Wayne State University, 645 Mullett, Detroit, MI 48226
147. Sciences and Engineering Library, University of Missouri, Serials Department, Columbia, MO 65201
148. Sciences and Engineering Library, Mississippi State University, State College, MS 39762
149. Sciences and Engineering Library, University of Nebraska - Omaha, Box 688, Downtown Station, Omaha, NE 68101
150. Sciences and Engineering Library, University of New Mexico, Albuquerque, NM 87106
151. Sciences and Engineering Library, University of Nevada, Reno, NV 89507
152. Sciences and Engineering Library, New York University, 4 Washington Place, New York, NY 10003
153. Sciences and Engineering Library, New York University, Courant Instit. of Mathematical Sciences (CIMS), 251 Mercer Street, New York, NY 10012
154. Sciences and Engineering Library, State University of New York Buffalo, Rotary Road, Buffalo, NY 14214
155. Sciences and Engineering Library, Ohio Wesleyan University, Delaware, OH 43015
156. Sciences and Engineering Library, Akron University, Akron, OH 44304
157. Sciences and Engineering Library, University of Cincinnati, Cincinnati, OH 45221
158. Sciences and Engineering Library, Oregon State University, Corvallis, OR 97331
159. Sciences and Engineering Library, University of Oregon, Eugene, OR 97403
160. Sciences and Engineering Library, Carnegie-Mellon University, Pittsburgh, PA 15213
161. Sciences and Engineering Library, University of Pittsburgh, Pittsburgh, PA 15213
162. Science and Engineering Library, Southern Methodist University, Hillcrest and University Blvd., Dallas, TX 75222
163. Sciences and Engineering Library, North Texas State University, Denton, TX 76203
164. Sciences and Engineering Library, University of Texas, Austin, TX 78712
165. Sciences and Engineering Library, Texas A and M University, College Station, TX 77843
166. Sciences and Engineering Library, Texas Tech University, Lubbock, TX 79409
167. Sciences and Engineering Library, Washington State University, Pullman WA 99163
168. Science and Engineering Library, Tulane University, New Orleans, LA 70112
169. Science and Engineering Library, Vanderbilt University, 24th Avenue South, Nashville, TN 37203
170. Science and Engineering Library, McGill University, Montreal, P.Q., Canada
171. Document Collection, Fondren Library, Rice University, 6100 Main Street, Houston, TX 77001
172. National Academy of Sciences, National Research Council, 2101 Constitution Ave., N.W., Washington, DC 20418
173. International Atomic Energy Agency, Karntner Ring 11, P.O. Box 590, A-1011 Vienna, Austria
174. Main Library, CERN, 1211 - Geneva 23, Switzerland

175-336. Given distribution as shown in TID-4500 for category UC-32.